A Conceptual Model for the Development of Tornadoes in the Complex Orography of the Po Valley

FRANCESCO DE MARTIN,[a,b] SILVIO DAVOLIO,[b,c] MARIO MARCELLO MIGLIETTA,[d,e] AND VINCENZO LEVIZZANI[b]

[a] *Department of Physics and Astronomy, Alma Mater Studiorum – University of Bologna, Bologna, Italy*
[b] *Institute of Atmospheric Sciences and Climate (CNR-ISAC), National Research Council of Italy, Bologna, Italy*
[c] *Dipartimento di Scienze Della Terra "A. Desio," Università Degli Studi di Milano, Milano, Italy*
[d] *Department of Earth and Geoenvironmental Sciences, University of Bari "Aldo Moro," Bari, Italy*
[e] *Institute of Atmospheric Sciences and Climate (CNR-ISAC), National Research Council of Italy, Padua, Italy*

(Manuscript received 1 October 2023, in final form 11 March 2024, accepted 18 March 2024)

ABSTRACT: The Po Valley in northern Italy is a hotspot for tornadoes in Europe in spite of being surrounded by two mountain ridges: the Alps in the north and the Apennines in the southwest. The research focuses on the case study of 19 September 2021, when seven tornadoes (four of them rated as F2) developed in the Po Valley in a few hours. The event was analyzed using observations and numerical simulations with the convection-permitting Modello Locale in Hybrid Coordinates (MOLOCH) model. Observations show that during the event in the Po Valley, there were two surface boundaries that created a triple point: an outflow boundary generated by convection triggered in the Alpine foothills and a dryline generated by downslope winds from the Apennines, while warm and moist air advected westward from the Adriatic Sea east (ahead) of the boundaries. Tornadoes developed about 20 km northeast of the triple point. Numerical simulations with 500-m grid spacing suggest that the development of supercells and drylines in the Po Valley was sensitive to the elevation of the Apennines. Simulated vertical profiles show that the best combination of instability and wind shear for the development of tornadoes was attained within a narrow area located ahead of the dryline. A conceptual model for the development of tornadoes in the Po Valley is proposed, and the differences between tornado environments over a flat terrain and over a region with complex terrain are discussed.

SIGNIFICANCE STATEMENT: The Po Valley is a highly populated area where some of the most violent tornadoes in Europe have developed. We investigated a tornado outbreak that occurred on 19 September 2021 in this region, in order to identify its main environmental characteristics. High-resolution numerical simulations revealed that values of instability and wind shear were compatible with the development of several tornadoes only in a narrow area close to the intersection of two surface boundaries (a triple point). Moreover, the atmospheric environment during the tornado outbreak was strongly influenced by the presence of mountain ridges surrounding the plain. We have summarized our results in a conceptual model that can potentially be used for forecasting applications.

KEYWORDS: Complex terrain; Tornadogenesis; Drylines; Severe storms; Mesoscale processes; Numerical analysis/modeling

1. Introduction

Tornadoes are an underestimated threat in Europe (Antonescu et al. 2017). Even if they are much less frequent than in the United States (232 tornadoes per year compared with 1223 tornadoes per year;[1] Taszarek et al. 2020a), the exposure and the vulnerability are high because significant tornadoes may occur over densely populated areas, where a dedicated warning system is still lacking (Miglietta and Rotunno 2016; Antonescu et al. 2017).

Italy is a hotspot for tornadoes in Europe (Fig. 1a of Antonescu et al. 2017): In the period 1950–2015, it is the European country with the highest economic losses and with the second highest number of injuries and fatalities caused by tornadoes (Table 1 of Antonescu et al. 2017). In Italy, tornadoes occur more frequently in the eastern Po Valley, along the Tyrrhenian coasts, and along the Ionian coast of Apulia region (Fig. 1a; Miglietta and Matsangouras 2018). Recent numerical studies investigated some violent tornado events along the latter two coastal areas (Miglietta et al. 2017a,b; Avolio and Miglietta 2021, 2022, 2023), but literature on tornado events in the Po Valley is scarce.

Taszarek et al. (2020b), using ERA5 reanalysis (Hersbach et al. 2020), showed that northern Italy is the European region with the most favorable conditions for severe storm development. In fact, the distribution of the 95th percentile of

[1] The areal extension of the two continents is nearly equivalent.

Denotes content that is immediately available upon publication as open access.

Supplemental information related to this paper is available at the Journals Online website: https://doi.org/10.1175/MWR-D-23-0222.s1.

Corresponding author: Francesco De Martin, francesco.demartin2@unibo.it

DOI: 10.1175/MWR-D-23-0222.1

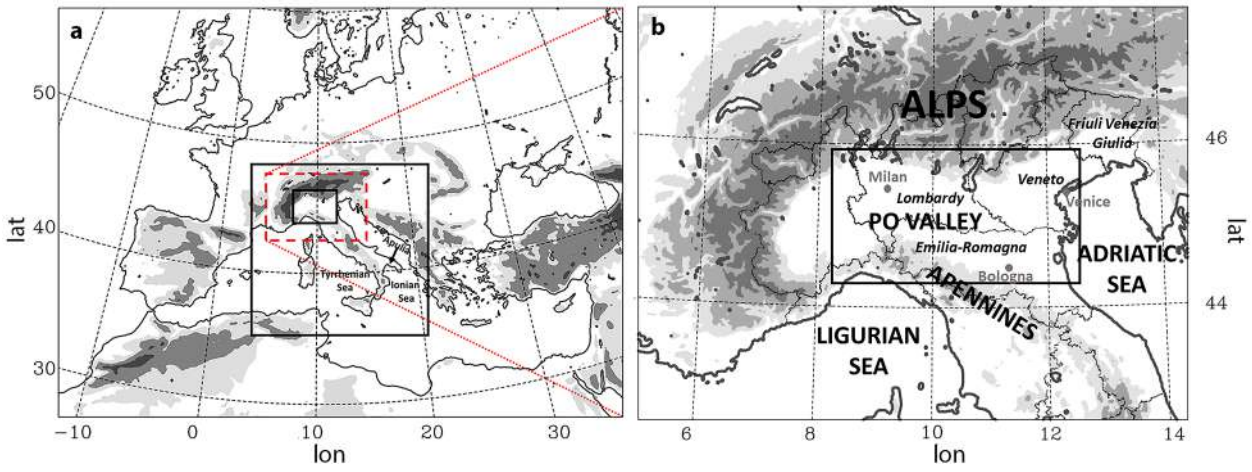

FIG. 1. (a) Orography and integration domain of the BOLAM simulation; the two black boxes highlight the domains of the two nested MOLOCH simulations, performed, respectively, at 1250- and 500-m grid spacing. (b) Orography of northern Italy [red box in (a)]; the box delimits the area of Figs. 3 and 4; names of regions and relevant locations mentioned in the text are also indicated. Gray shading for orography elevation corresponds to 500, 1000, and 2000 m.

the parameter MLWMAXSHEAR = $\sqrt{2\text{MLCAPE}} \times \text{BS}_{0-6\text{km}}$ (where MLCAPE is the mixed layer convective available potential energy and $\text{BS}_{0-6\text{km}}$ is the 0–6-km bulk shear) and of the significant tornado parameter (STP; Thompson et al. 2003) peaks in this area, where the highest number of hours with lightning is also observed.

While tornadoes are generally disadvantaged over mountain regions (Markowski and Dotzek 2011), tornadogenesis can be promoted in the surrounding valleys, where low-level circulations forced by topographic features can increase instability and wind shear (Feldmann et al. 2024; Matsangouras et al. 2016; Bosart et al. 2006; Homar et al. 2003; Bluestein 2000). This is the case of northern Italy, where tornadoes do not usually develop over the mountains, but in the nearby plains, which are surrounded by the complex orography of the Alps and of the Apennines (Fig. 1b). In this region, tornadoes are much more frequent than in other flat European areas (Fig. 1a of Antonescu et al. 2017), suggesting that the peculiar topography of northern Italy may favor tornadogenesis. A few studies found that low-level circulations generated by the Alps and the Apennines influenced severe storm development in the nearby plains of northern Italy (Pichelli et al. 2017; Davolio et al. 2016; Miglietta et al. 2016), but poor attention was given to tornado events so far. Only very few observational studies investigated weak tornado events in the region (see Miglietta and Matsangouras 2018 for a review), and we believe further attention is needed.

Bagaglini et al. (2021), hereafter B21, made a similar analysis of Taszarek et al. (2020b) using ERA5 over 19 years, but only for days with F1+ tornadoes in five different regions of Italy. In their study, northeast (NE) Italy emerged as the region with the most numerous clusters (51 events out of 149). There, they found values of CAPE (about 800 J kg^{-1}) comparable with those observed in tornado days in the other analyzed Italian regions, although significantly smaller than the CAPE values observed in the United States. On the other hand, on tornado days, low-level wind shear in the Po Valley is significantly weaker [low-level shear (LLS) around 5 m s^{-1} and storm relative helicity (SRH) from surface to 900 hPa less than 50 m^2 s^{-2}] than the values observed in the other clusters analyzed in that study, as well as in other parts of Europe (Púčik et al. 2015) and in the United States (Thompson et al. 2003). Ingrosso et al. (2020) attained a similar result restricting the analysis to F2+ Italian tornadoes only.

The reason why ERA5 identifies low values of low-level wind shear in the Po Valley during tornado events requires further investigation. This question is even more intriguing and relevant since LLS and low-level SRH are among the most skillful parameters to distinguish between weak and significant tornadoes (Thompson et al. 2003) and since some of the most violent (and deadliest) tornadoes in Europe developed in the area (Groenemeijer and Kühne 2014).

The present paper deals with the issue of tornado-prone environments over northern Italy, analyzing the significant tornado outbreak that occurred on 19 September 2021: In a few hours, seven tornadoes (four of them rated as F2) developed between the Lombardy and Emilia Romagna regions (Fig. 1b). The event presented similar environmental characteristics to those found by B21. However, while B21 employed a statistical approach, here we want to investigate in more detail the tornadic environment and the dynamical processes of a specific event by means of observations and high-resolution numerical simulations. An explanation for the development of (even violent) tornadoes in the Po Valley, despite the seemingly unfavorable conditions described by ERA5, is proposed, demonstrating the role of surface boundaries and of the complex orography in influencing the severe storm dynamics.

The paper is organized as follows. Section 2 provides a synoptic overview of the event and an analysis of the available observations. Section 3 describes the numerical simulation

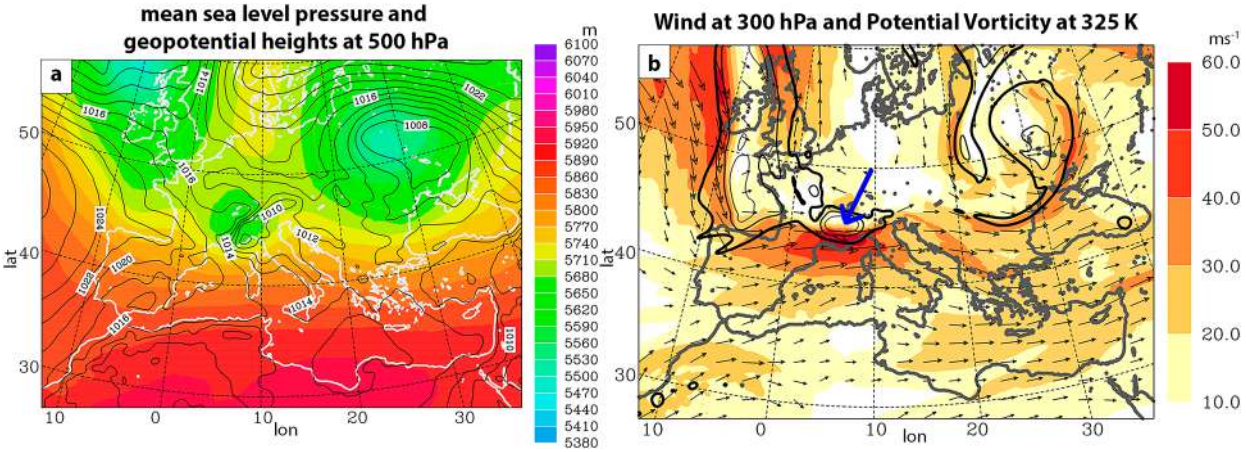

FIG. 2. ECMWF analysis of 1200 UTC 19 Sep 2021. (a) Geopotential height at 500 hPa (m; color shading) and mean sea level pressure (hPa; contours); (b) wind at 300 hPa (vectors and color shading; m s^{-1}) and PV at 325 K (contours). PV contours correspond to 2 PVU (thickest) and 5 and 10 PVU (thinnest) (1 PVU = 10^{-6} K kg^{-1} m^2 s^{-1}). The blue arrow indicates the PV maximum in the Western Alps. The plotted domain is the same as in Fig. 1a.

setup based on the Bologna Limited-Area Model (BOLAM)–MOLOCH modeling chain. Section 4 analyzes the numerical results, focusing on the role of the Apennines and of the surface boundaries in the development of supercells and tornadoes. A comparison between the tornadic environments described by ERA5 and MOLOCH is also performed in section 4. In section 5, a conceptual model for the development of tornadoes in the Po Valley is proposed, and finally, conclusions are drawn in section 6.

2. Observations

a. *Synoptic analysis*

On 19 September 2021, a cutoff low at 500 hPa, with an attendant surface low pressure system, entered the Po Valley from France (Fig. 2a) and crossed northern Italy from west to east. The cutoff low was associated with an intense upper-level anomaly of potential vorticity (PV; blue arrow in Fig. 2b). The 300-hPa jet streak was located between southern France and the Ligurian Sea, with a marked region of diffluence above the Po Valley. The supercells and tornadoes developed in the left exit region of the jet streak, in the eastern side of the PV anomaly, a typical location for tornado outbreaks (Rose et al. 2004; Tochimoto and Niino 2016; Tochimoto et al. 2021).

b. *Surface observations and radar analysis*

In Figs. 3 and 4, hourly station data and radar reflectivity are plotted,[2] while in Table 1 the tornadoes are summarized in terms of pathlength, rating, and time, as reported in the European Severe Weather Database (ESWD). A complete damage survey can be found in Pavan (2022).

[2] In the supplemental material S1, a radar animation of the event with frames every 5 min is also provided.

In the first hours of 19 September 2021, a quasi-stationary mesoscale convective system (MCS) was positioned over the Western Alps (Fig. S2 in the online supplemental material), a well-known hotspot for convective initiation (Manzato et al. 2022). Then, around 1000 UTC a quasi-linear convective system (QLCS) developed in the Po Valley (Fig. 3a), possibly triggered by the outflows of the MCS in the Alps and by the increasing upper-level forcing. The QLCS generated an outflow boundary, while in the eastern part of the plain there was a moist and warm southeasterly flow. The outflow boundary was characterized by a backing of the wind from east to north and by a slight decrease in temperature (about 2°C). On the other hand, south of Piacenza, a drier flow descending from the Apennines (Fig. 3b) created a dryline. It was characterized by a veering of the wind from east to southwest, by a slight increase in temperature (about 2°C), and by a gradient of dewpoint temperature from 5°C (20 km)$^{-1}$ in the initial stages up to 11°C (15 km)$^{-1}$ at 1300 UTC.

It is worth noting that the dryline was initially confined in a narrow region on the lee of the western Apennines, with a bulge shape (Fig. 3b), and then, it extended eastward in the afternoon (Figs. 3c and 4). This is due to the progressive eastward displacement of a dry southwesterly flow above the Ligurian Sea, associated with the upper-level forcing (that point is further stressed by the numerical results in section 4b).

The QLCS moved eastward, and around 1100 UTC (Fig. 3b), its southern part dissipated, possibly due to the interaction with the dry air descending from the Apennines. Consequently, storm number 1 (Fig. 3b) strengthened south of Milan, generating the first tornado near Roncaro at 1115 UTC, rated as F1. We believe that storm number 1 was a supercell, at least after 1200 UTC, but there are no Doppler radars available in the region to confirm this hypothesis. However, some photographic reports suggested the presence of a mesocyclonic circulation (a wall cloud and a clear slot associated with the rear flank downdraft were spotted; Signani 2021). It remained isolated for a very long period

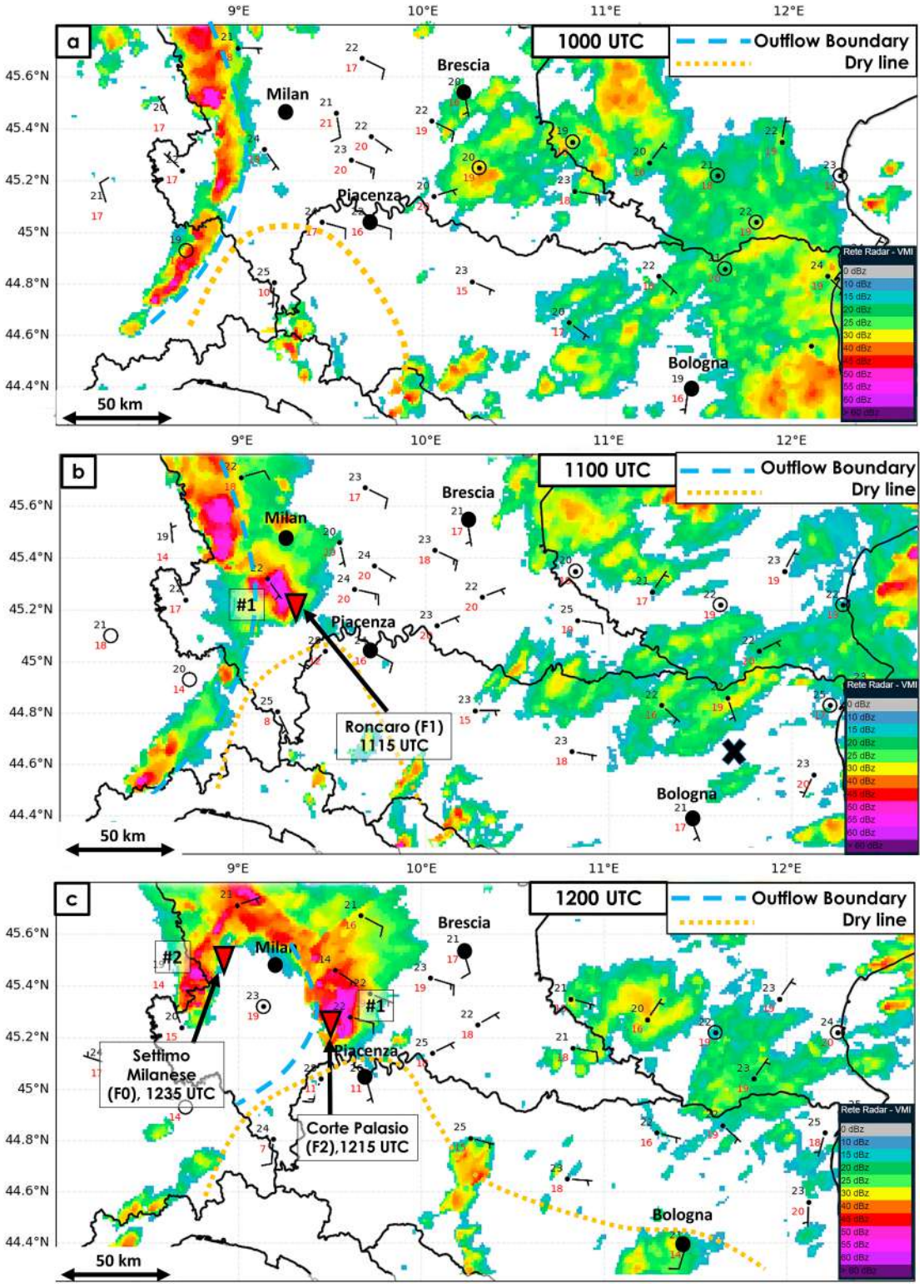

FIG. 3. Observations of temperature (black numbers; °C), dewpoint temperature (red numbers; °C), and wind (barbs) at ground stations; maximum radar reflectivity (dBZ) at (a) 1000, (b) 1100, and (c) 1200 UTC 19 Sep 2021. The plotted domain is highlighted with a black box in Fig. 1b. The tornadoes that occurred closest in time to the hourly time step are identified with a red triangle, and the affected villages are indicated. The dryline (dashed yellow) and outflow boundary (dashed blue) locations are subjectively identified. In (b), the cross indicates the location of the atmospheric sounding in Fig. 5. Weather station data were provided by the Environmental Agencies of Emilia Romagna, Lombardy, Piedmont, and Veneto regions, while the radar images were provided by the Civil Protection Department of Italy.

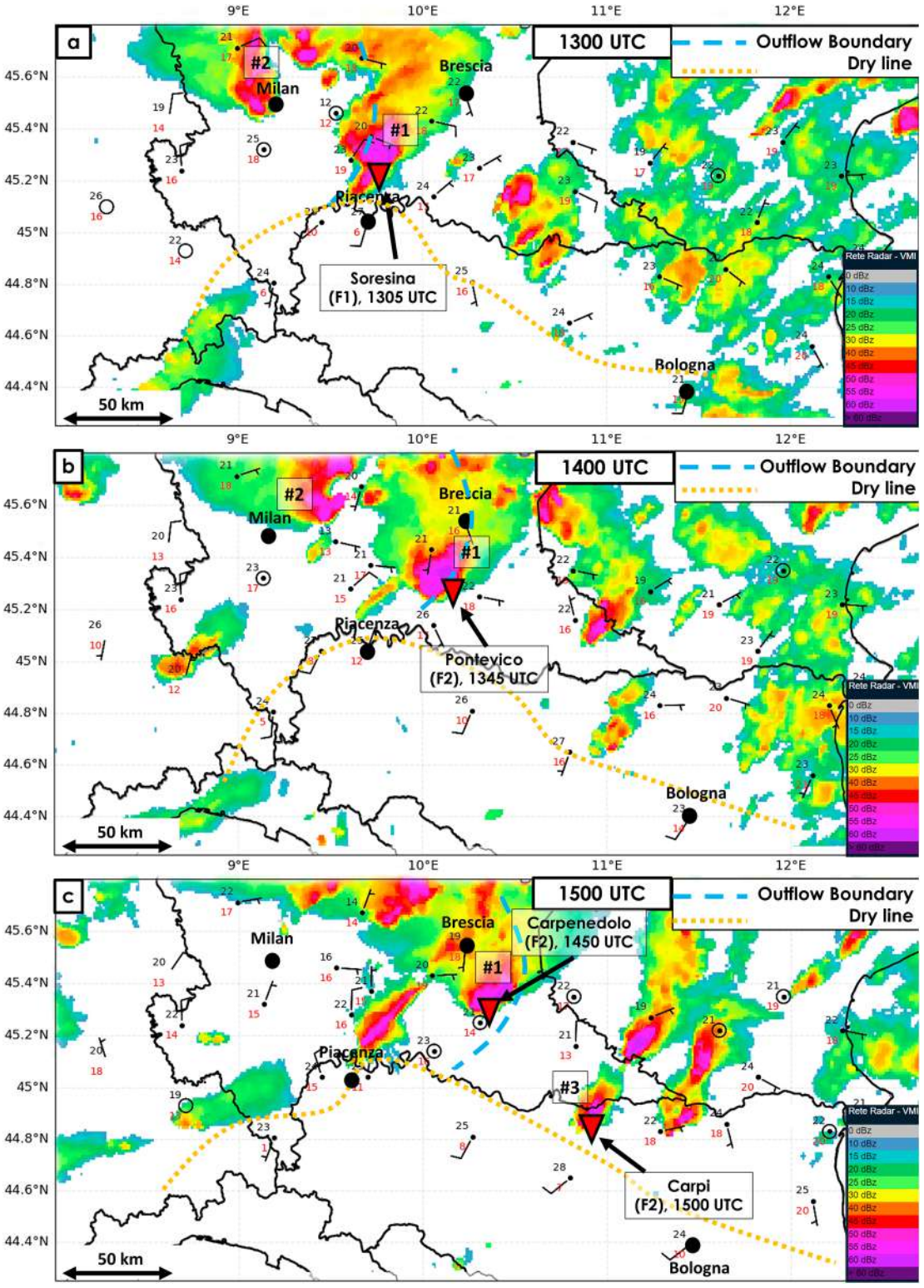

FIG. 4. As in Fig. 3, but at (a) 1300, (b) 1400, and (c) 1500 UTC 19 Sep 2021.

TABLE 1. Characteristics of the tornadoes developed on 19 Sep 2021 (source ESWD).

Place	Rating	Pathlength (km)	Time UTC
Roncaro	F1	2.8	1115
Corte Palasio	F2	2.2	1215
Settimo Milanese	F0	0.4	1235
Soresina	F1	3.3	1305
Pontevico	F2	6.2	1345
Carpenedolo	F2	7.1	1450
Carpi	F2	4.7	1500

(7 h), deviating from the mean wind with frequent inflow notches (see the animation in the supplemental material S1), and generated multiple F1+ tornadoes. It may be considered as the first long-lived supercell studied in Italy.

It moved eastward, a few kilometers north of the dryline, and at 1215 UTC, it generated a second tornado near Corte Palasio (Fig. 3c), rated as F2. A multicell storm west of Milan (storm number 2 in Fig. 3c) generated another weak tornado (F0) near Settimo Milanese at 1235 UTC. At 1305 UTC, storm number 1 spawned a tornado near Soresina (rated as F1; Fig. 4a), close to the dryline bulge, on the north side of the strong gradient of dewpoint temperature (about 11°C in 15 km) near Piacenza (Fig. 4a).

Then, the initial outflow boundary weakened (Fig. 4b). Storm number 1 generated two further significant tornadoes near Pontevico (at 1345 UTC; Fig. 4b) and near Carpenedolo (at 1450 UTC; Fig. 4c), both rated as F2 and with pathlength of 6.2 and 7.1 km, respectively (Table 1). Between 1300 and 1500 UTC, hailstones were also reported below that storm (5 cm in diameter near Pontevico). Finally, storm number 1 moved into the Veneto region, where it started to weaken until its dissipation east of Verona around 1730 UTC.

At 1440 UTC, a new storm (storm number 3 in Fig. 4c) developed not far from Bologna: Likely, it was another supercell (Poli and Stanzani 2021), and it generated the last tornado of the day at 1500 UTC near Carpi, rated as F2. The convective system (Fig. 4c), composed of multiple convective cells, moved eastward into the Veneto and Friuli–Venezia Giulia (FVG) regions in the evening, causing hailstorms and heavy rain, and it finally dissipated during the night.

c. *Atmospheric sounding*

The atmospheric sounding in S. Pietro Capofiume (Fig. 5; location indicated in Fig. 3b) sampled an area about 200 km

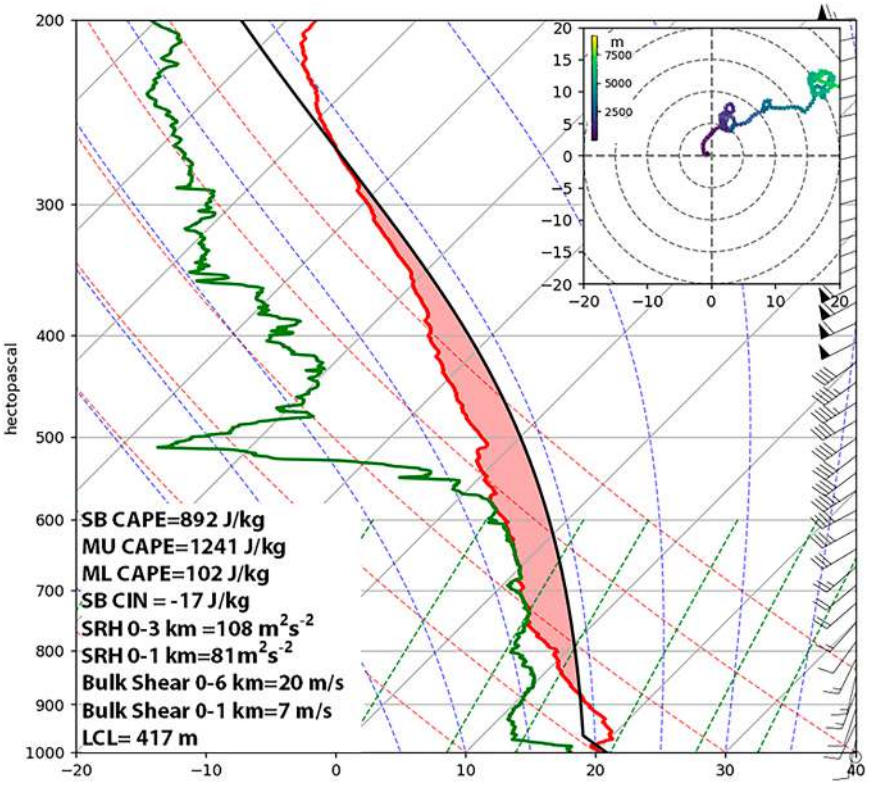

FIG. 5. Atmospheric sounding observed in S. Pietro Capofiume (location indicated with a cross in Fig. 3b) at 1200 UTC 19 Sep 2021: Dewpoint temperature (green line), temperature (red line), and surface-based parcel profile (black line) are shown. On the right, wind barbs are plotted [half barb (2.5 m s^{-1}), full barb (5 m s^{-1}), and flag (25 m s^{-1})]. In the upper right part of the figure, the hodograph is shown: colors change according to height—violet (surface) and green (5000 m AGL). Indexes are computed following May et al. (2022).

away from the tornadic storm. It is representative of the warm and moist air mass in the eastern part of the plain, even if, at that location, the surface flow was more southerly than in the area where tornadoes developed (where a southeasterly flow was present at the surface).

The southerly flow was very shallow and moist, while a capping inversion [surface-based (SB) convective inhibition (CIN) = -17 J kg^{-1}], due to the drier and warmer southwesterly flow, was just above. The almost saturated air mass near the surface was possibly a consequence of light rainfall that occurred just before the launch of the sounding (Fig. 3a). In the upper levels, the strong westerly jet observed in Fig. 2b is clearly shown. The most unstable (MU) CAPE was moderate (1241 J kg^{-1}), as well as the 0–6-km bulk shear (20 m s^{-1}), while the SRH was quite low (81 m^2 s^{-2} in the 0–1-km layer). The SB lifting condensation level (LCL) was very low (417 m) due to the high values of moisture at the ground.

Although this sounding reveals an environment favorable for the development of supercells, it is not the typical atmospheric sounding of a tornado outbreak, due to the quite low values of wind shear near the ground. However, it is likely that the vertical thermodynamic and wind profiles closer to the storm were different. In fact, close to the supercell (e.g., north of Piacenza in Fig. 3b) surface winds were more backed (easterly), possibly associated with stronger low-level SRH than in the location where the sounding was launched. The high amount of moisture at the ground in the sounding is known as an important element for tornadogenesis (Thompson et al. 2003).

d. *Considerations about the surface boundaries*

As revealed by the surface and radar observations, the dryline probably triggered the isolated supercell number 3 responsible for the tornado near Carpi (Fig. 4c), while the long-lived supercell number 1 was probably triggered by the outflow boundary (Fig. 3b). Hence, the severe storms developed close to the intersection between the dryline and the outflow boundary: To the knowledge of the authors, it is the first evidence of a triple point in Europe. However, there are some differences with respect to the typical U.S. triple points:

- The spatial scale of the dryline and of the outflow boundary was much smaller than in the United States (Hoch and Markowski 2005). This is probably due to the complex orography of the region: The Alps in the north and the Apennines in the south limit the extension of the surface boundaries.
- In the United States, drylines are almost linear with a north–south orientation and the origin of the dry air is associated with the northeastward advection of a continental tropical air mass. In this case, the dryline was initially a bulge (Fig. 3c), and then, it expanded eastward (Fig. 3c). It was generated by the advection of a dry air mass from the southwest and by an adiabatic compression in the lee side of the Apennines (this aspect is explored further in section 4b). The different orientation of the mountain ridge with respect to the Rocky Mountains probably influenced the different dryline's orientation.
- All the tornadoes, except that of Settimo Milanese, developed very close to the dryline (within 10–20 km of distance). The storms that developed far away from the dryline did not produce tornadoes.

The suitable conditions for tornadoes were probably attained only close to the dryline, while just some tens of kilometers away from it the environment was no longer supportive. In the United States, a similar behavior was observed in the case of thermal boundaries, where supercells generated tornadoes on the cool side of the surface boundary (Rasmussen et al. 2000; Markowski et al. 1998; Atkins et al. 1999). Instead, in the present case, the long-lived supercell was triggered by the outflow boundary, and then, it moved into the moist and warm air mass where it generated the tornadoes. Hence, this case study looks somewhat different with respect to the events analyzed in the United States, and numerical simulations were performed to better assess the role of the surface boundaries.

3. Numerical simulations

a. *Model setup*

Numerical simulations of the severe event were performed with the modeling system consisting of the hydrostatic BOLAM (Buzzi et al. 2003) and the nonhydrostatic, fully compressible, convection-permitting model MOLOCH (Malguzzi et al. 2006; Davolio et al. 2017). The two models are employed in cascade (one-way nesting) and have been developed at the Institute of Atmospheric Sciences and Climate of the National Research Council of Italy (CNR-ISAC). A detailed description of the models and their applications can be found in Buzzi et al. (2014) and Davolio et al. (2020). In the following, only a brief and general description of MOLOCH is provided, since the results discussed here are based mainly on high-resolution simulations, while BOLAM is exploited only to provide lateral boundary conditions at the appropriate spatial resolution and hourly frequency.

MOLOCH employs a staggered Arakawa C grid and a height-based hybrid coordinate, relaxing smoothly to horizontal surfaces away from Earth's surface. The prognostic variables are pressure, virtual temperature, specific humidity, horizontal and vertical wind velocity components, turbulent kinetic energy, and five water species defined in the microphysical parameterization scheme. For the time integration, a time-split scheme with an implicit treatment of the vertical propagation of sound waves is applied, while a forward–backward scheme is implemented for the horizontal propagation of gravity and sound waves. The three-dimensional advection is computed by a second-order, weighted-average flux implementation with superbee limiter (Hubbard and Nikiforakis 2003). The physical package includes an eddy kinetic energy–mixing length (E–l) 1.5-order closure (Trini Castelli et al. 2020) for the boundary layer turbulence, a 7-layer soil model, and a microphysical scheme, described in Buzzi et al. (2014). The atmospheric radiation is computed through a combined application of the Ritter and Geleyn (1992) and the ECMWF (Morcrette et al. 2008) schemes.

b. Numerical experiments

Different initial and boundary conditions provided by the Integrated Forecasting System (IFS) global model were used to initialize the BOLAM, which was implemented with a grid spacing of 8.3 km in the domain of Fig. 1a. Then, MOLOCH was nested in the BOLAM simulation, with a grid spacing of 1250 m. A further MOLOCH simulation at 500-m grid spacing (domains in Fig. 1a) was nested in the 1250-m spacing run. The simulation initialized with the IFS forecast at 0000 UTC 19 September 2021 was selected as the "control run" because it reproduced better the thunderstorm evolution[3] shown in Figs. 3 and 4.

In addition to the control run, further experiments were performed to test the sensitivity of the results to some environmental characteristics (Table 2). Two tests were performed using a modified orography of the Apennines, respectively, halved (orog50) or increased by a factor of 1.5 (orog150), in the inner MOLOCH domain with grid spacing of 500 m. The meteorological initial fields over the modified orography were obtained by interpolation between the levels of the outer model fields in orog150 and by extrapolation from the bottom levels of the outer model in orog50. The latter is performed keeping the modeled lapse rate, but smoothing with a fixed climatological lapse rate in order to avoid unrealistic profiles. In any case, the model rapidly adjusts possible noise in the surface fields.

Another test (bm60) was performed, aimed at understanding the possible role of the large-scale advection of dry air from the southwest for the development of supercells in the Po Valley. The boundary condition was modified along the southwestern portion of the domain: Here, the specific humidity below 3000 m above ground level (AGL) was increased, to reach a relative humidity of 60% at least (no modification was done wherever the relative humidity was higher). Above 5000 m AGL, the specific humidity was not perturbed, while between 3000 and 5000 m AGL the specific humidity was relaxed by means of a linear function from the perturbed values at 3000 m AGL to the value of the control run at 5000 m AGL. The moisture increase was limited to 60% to avoid condensation and precipitation over the Apennines crest.

4. Results

This section is divided into three main parts. First of all, in section 4a the mesoscale environment where the supercells developed is described using the control run. In the same section, the sensitivity of the environment to the southwesterly flow crossing the Apennines is investigated by means of the numerical sensitivity experiments orog50 and orog150. Second, in section 4b, the role of the surface boundaries, in particular of the dryline, in forging a favorable tornadic environment is deeply investigated. Finally, in section 4c, the skill of ERA5 reanalysis in the description of the tornadic environment is assessed.

[3] In the supplemental material S3, radar reflectivity produced by the control run is provided.

TABLE 2. Simulations performed with a 500-m horizontal grid spacing inside the inner box in Fig. 1a. The first one is the control run, and others are the sensitivity tests.

Simulation name	Characteristic
Control	Unperturbed simulation
orog50	Apennines orography halved
orog150	Apennines orography increased by a factor of 1.5
bm60	Humidity in the southwestern boundary increased

a. Role of the Apennines orography in supercell development

The control simulation shows that during the morning of 19 September 2021, a tongue of moist and warm air, characterized by high values of dewpoint temperature at the surface (Fig. 3) and of θ_e at 950 hPa (Fig. 6a), extends from the Adriatic Sea toward the Lombardy Region. It is associated with moderate values of SB CAPE (>1200 J kg^{-1}) and SRH 0–3 km (average of 200 m^2 s^{-2}; Fig. 6b), due to the veering of the wind from southeasterly near the surface to southwesterly above 850 hPa (not shown). As shown in Miglietta et al. (2016), the high θ_e tongue from the Adriatic Sea may be important for supercell development in the Po Valley, being associated with both high values of instability and directional wind shear. Here, the area presenting a favorable combination of CAPE and SRH (Fig. 6b) is quite narrow, much smaller than those typically observed in tornadic outbreaks in the United States (Tochimoto and Niino 2016), but sufficient for the development of a long-lived tornadic supercell.

The presence of the high θ_e tongue appears relevant to promote intense convection, and its location is modulated by the interaction with the southwesterly flow descending from the Apennines. That interaction is explored through two sensitivity experiments, orog50 and orog150, described in section 3b.

The dynamic characteristics of the southwesterly flow from the Apennines can be described by the inverse of the Froude number, which is the ratio between the product of the upstream Brunt–Väisälä frequency and the characteristic mountain height h, and the impinging wind speed. Figure 7 shows that in the control run the southwesterly flow is in an intermediate regime during the day, since the Froude number oscillates around the value of 1, while in the orog50 (orog150) simulation, a clear flow-over (flow-blocked) regime occurs. It is worth saying that the value of the Froude number does not depend significantly on the selected position over the Ligurian Sea, upstream of the Apennines orography.

Reducing the Apennines elevation (flow-over regime), the southwesterly flow enters farther north over the plain (Fig. 6c) so that the directional shear and the SRH are reduced in the Po Valley and slightly increased on the Alpine foothills (Fig. 6d). Moreover, the high θ_e tongue and the area with high values of CAPE > 1200 J kg^{-1} become narrower and slightly shifted to the north. The resulting combination of CAPE and SRH is less favorable for the development of supercells in the Po Valley in

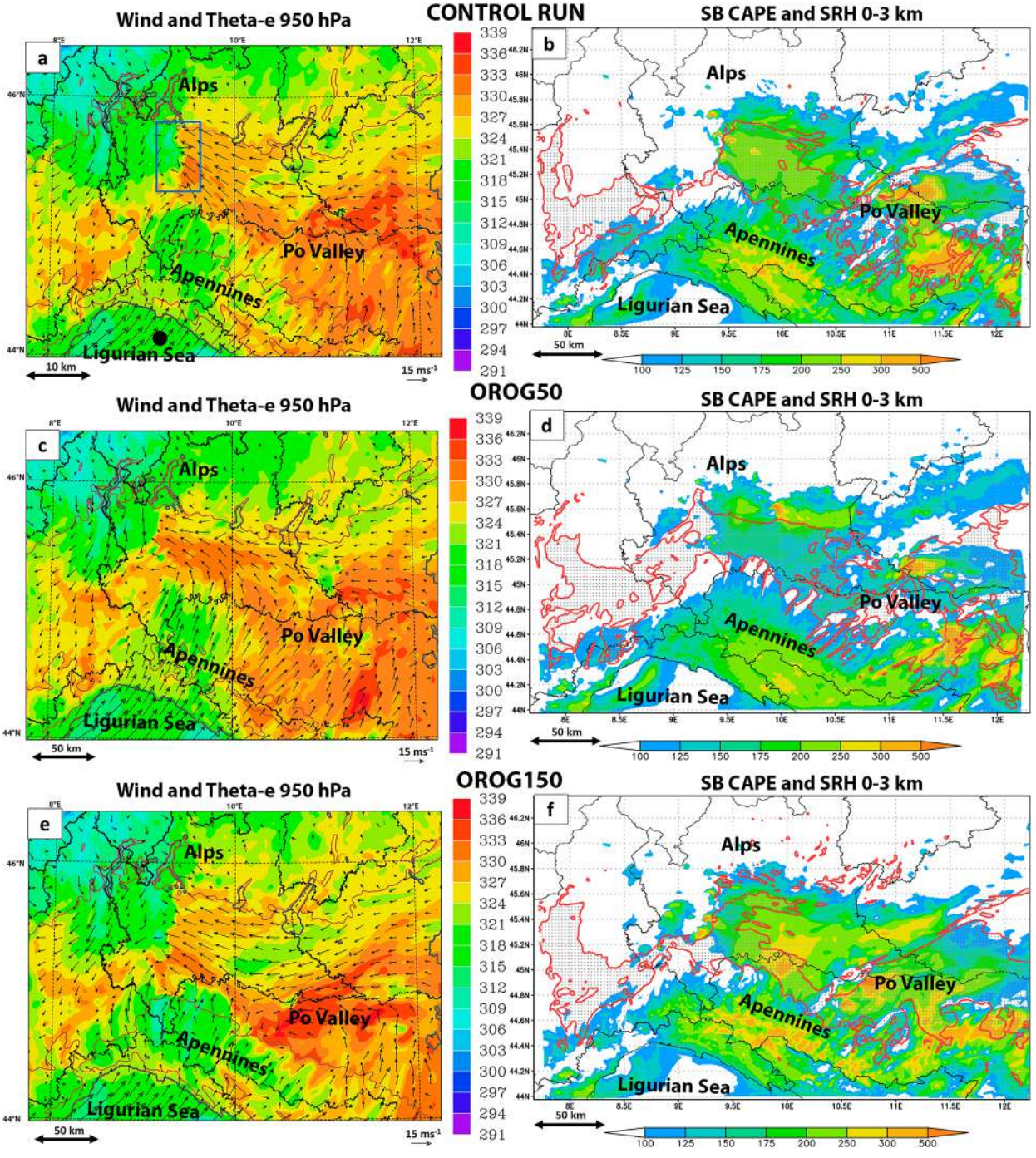

FIG. 6. Control simulation at 1300 UTC 19 Sep 2021: (a) wind speed (m s^{-1}; vectors) and θ_e (K; color shading) at 950 hPa; (b) SRH 0–3 km (m^2 s^{-2}; shaded) and contour of 1200 J kg^{-1} of SB CAPE (highlighted by hatching). (c),(d) As in (a) and (b), but for orog50 experiment (reduced Apennines orography); (e),(f) as in (a) and (b), but for orog150 experiment (increased Apennines orography). The reference length of the wind vectors is indicated at the bottom right. The thin brown contour line in (a), (c), and (e) indicates the 500-m isoline for the orography. The plotted domain corresponds to the inner box in Fig. 1a. The black dot in (a) indicates the position where the Froude number is computed. The blue box in (a) indicates the domain shown in Fig. 11.

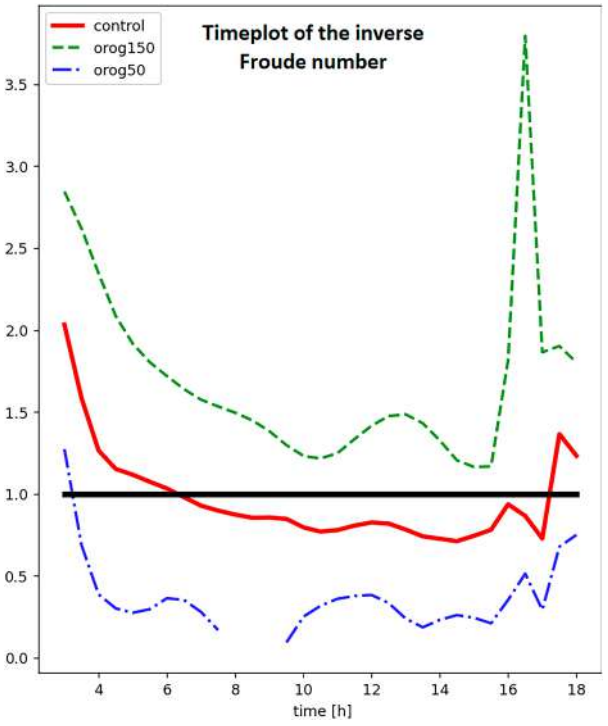

FIG. 7. Timeplot of the inverse Froude number computed over the Ligurian Sea, for the three numerical simulations: control run (red), orog50 (blue), and orog150 (green). The reference value, corresponding to the flow regime transition, is highlighted with a black line. The location where the parameter is calculated is indicated by a black dot in Fig. 6a.

the orog50 experiment than in the control run. On the contrary, by increasing the Apennines elevation (flow-blocked regime), the easterly wind from the Adriatic Sea is allowed to flow closer to the Apennines foothills (Fig. 6e). Consequently, the peak of SRH and the tongue of high θ_e values and CAPE are shifted southward, closer to the Apennines foothills.

The different evolution of the dryline in the three experiments can be clearly appreciated in Fig. 8. This figure also shows that, conversely, the different elevation of the Apennines does not perturb the outflow boundary.[4] It was generated in the western Alpine foothills (Fig. 8a), and then, it propagated eastward, crossing all the Po Valley by the end of the day (Figs. 8d,g,j). The small sensitivity of the outflow boundary to the Apennines elevation is reasonable, since it is originated close to the Alps, whose elevation is not modified in the experiments, and since the storm dynamics are driven by an upper-level synoptic forcing.

Figure 9 summarizes the outcomes of the numerical experiments orog50 and orog150. The sketches show that the extent of the tongue of warm and moist air depends upon the elevation of the Apennines, while the outflow boundary is insensitive to these changes. Consequently, the interaction between the outflow boundary and the high θ_e–SRH tongue differs among the three experiments: In orog50, the outflow boundary reaches the warm and moist air mass later than in the control run and more to the north, while in orog150 the outflow boundary crosses the tongue earlier and closer to the Apennines foothills. Therefore, the supercell development is modified, as can be observed in Fig. 10.[5] In the control run (Fig. 10a), high values of updraft helicity (UH) reveal three different supercells (tracks highlighted with black vectors); in orog150 (Fig. 10b), a supercell is simulated in the southwestern part of the domain; and in orog50 (Fig. 10c), there are some isolated maxima of UH but not a clear supercell track. The time evolution of the UH maxima within the area highlighted with a black box in Fig. 9 is shown in Fig. 10d. In the control run (red line), UH reaches high values between 1100 and 1600 UTC, in the orog50 simulation (blue line) later, between 1330 and 1630 UTC, and in the orog150 simulation (green line) earlier, between 1100 and 1330 UTC. Analyzing together Figs. 9 and 10d, it turns out that supercells develop only when the outflow boundary crosses the high θ_e–SRH tongue. Moreover, in the orog50 scenario (Fig. 10c), a supercell track is not evident probably due to the less favorable combination of SRH and CAPE observed in Fig. 6d.

This analysis suggests that in the present case study the Froude number characterizing the southwesterly flow over the Ligurian Sea is a relevant parameter to identify conditions favorable for the development of supercells in the Po Valley. Depending on the flow regime, the location and strength of the high θ_e–SRH tongue from the Adriatic Sea are displaced, causing different supercell evolutions. In the presence of the high θ_e–SRH tongue, values of the inverse of the Froude number much higher than 1 are associated with supercell development close to the Alpine foothills, while values much less than 1 allow the development of supercells closer to the Apennines foothills. The strong sensitivity of the severe storms to small uncertainties in the Froude number when its value is around 1 may contribute to explain the limited model skills of numerical simulations of supercells (Miglietta et al. 2016; Pilguj et al. 2022) and squall lines (Pichelli et al. 2017) in northern Italy, since slightly different wind speed crossing the Apennines can significantly change the severe storm behavior in the valley.

b. *The role of the surface boundaries in the development of tornadoes*

After having clarified the effect of the Apennines on the southwesterly flow and in turn on the warm and moist tongue from the Adriatic Sea, the role of surface boundaries, in particular of the dryline, for the development of supercells is investigated in the following.

All the tornadoes were generated very close to the outflow boundary, along which the model simulates horizontal vorticity in the lower layers in correspondence of the gradient of

[4] At 1400 UTC in orog50, there is a delay in the progression of the outflow boundary (Fig. 8h), but at 1600 UTC it is aligned again with the other simulations (Fig. 8k).

[5] In the supplemental material, the simulated radar reflectivity of those simulations is provided in S4 and S5.

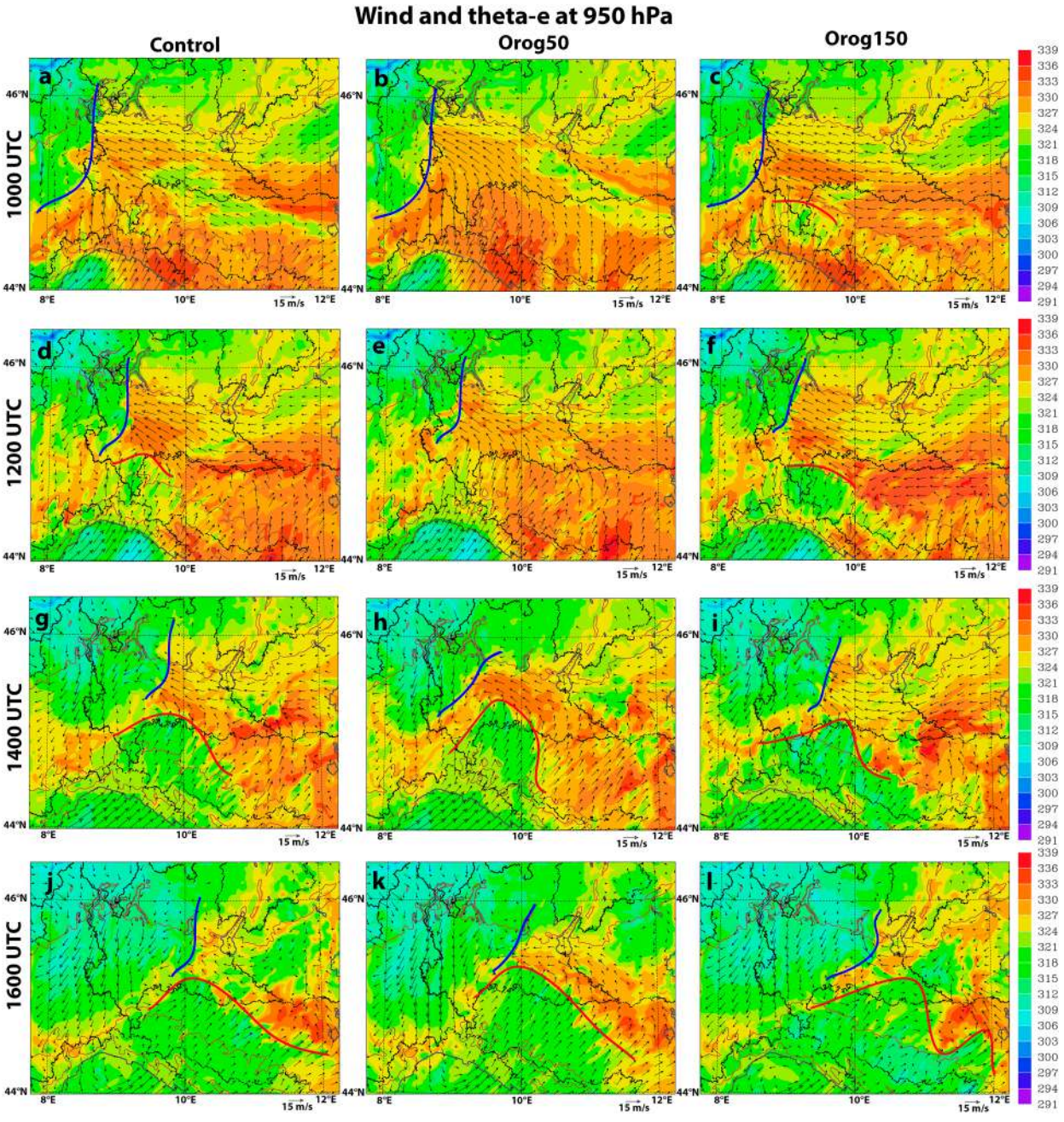

FIG. 8. Wind speed (m s^{-1}; vectors) and θ_e (K; color shading) at 950 hPa on 19 Sep 2021 for the control run at (a) 1000, (d) 1200, (g) 1400, and (j) 1600 UTC. The same plots are reported for the (b),(e),(h),(k) orog50 experiment and (c),(f),(i),(l) orog150 experiment. The outflow boundary and the dryline are highlighted, respectively, with blue line and red line. The reference length of the wind vectors is indicated at the bottom right. The thin brown contour line indicates the 500-m isoline for the orography. The plotted domain corresponds to the inner box in Fig. 1a.

potential temperature (Fig. 11a). The presence of streamwise vorticity along the outflow boundary is likely due to baroclinic generation, and the location of the intense updraft of the supercell (Fig. 11b) is consistent with the possible tilting of this baroclinic vorticity into the storm (Rotunno and Klemp 1985; Markowski and Richardson 2014).

Moreover, almost all tornadoes developed within 20 km from the dryline. The control run provides a credible simulation of the triple point (Fig. 12a), where the moist easterly flow from the Adriatic Sea in the Po Valley encounters the dry southwesterly flow from the Apennines and the cooler northerly flow from the Alps. The dryline was initiated by the

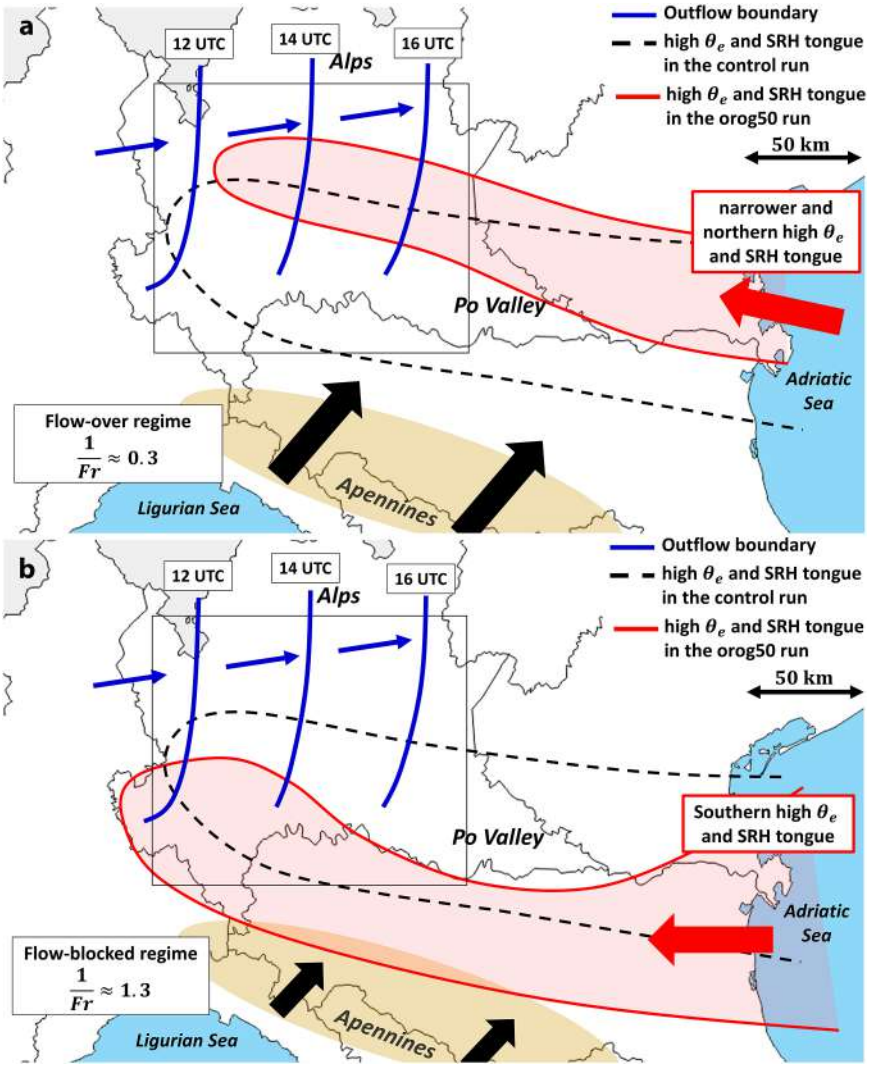

FIG. 9. Effect of variations of the Apennines elevation (and thus of the Froude number) on the location of high θ_e–SRH tongue (red line and shading) with respect to the control run (black dashed line). While the outflow boundary (blue line) moves during the afternoon, the unstable tongue remains quasi-stationary. (a) orog50 scenario (flow-over regime); (b) orog150 scenario (flow-blocked regime). The black box indicates the area over which max UH values are computed (see Fig. 10).

advection of a dry air mass from the southwest between 1000 and 1200 UTC (Figs. 8a,d). The dryline was first generated in a narrow region located about 45°N, 9.5°E (Fig. 8d; in good agreement with observations provided in Fig. 3c), and then, it moved eastward. The vertical section at 1400 UTC in Fig. 12b shows that just above the Ligurian Sea the southwesterly flow is characterized by relative humidity around 50%, but it becomes very dry (<10%) above 1000 m from the surface. The dryline was generated by both the advection of a dry air mass from the southwest and the adiabatic compression that occurred in the lee of the Apennines, similarly to what was found by Bechis et al. (2022) for a dryline in Argentina.

The numerical experiments varying the Apennines orography (orog50 and orog150, respectively; Figs. 12c,d) highlight the effect of adiabatic compression in the lee of the Apennines and the different propagation of the dry air in the Po Valley. With lower mountain elevation, the drying of the air is reduced, but the dry air penetrates farther north since the flow-over regime (section 4a) allows widespread downslope winds. The opposite is shown for higher orography: The flow is blocked upstream, but the adiabatic drying in the lee is increased.

Using the control run, some thermodynamic and wind shear indices were computed across the dryline and plotted as a function of the distance from the dryline itself (Fig. 13). The dryline is characterized by a strong vertical gradient of θ_e in the first kilometer of the atmosphere, surmounted by the dry southwesterly flow with low values of θ_e (Fig. 13a). About 10 km ahead of the dryline (negative values of x), in the warm–moist

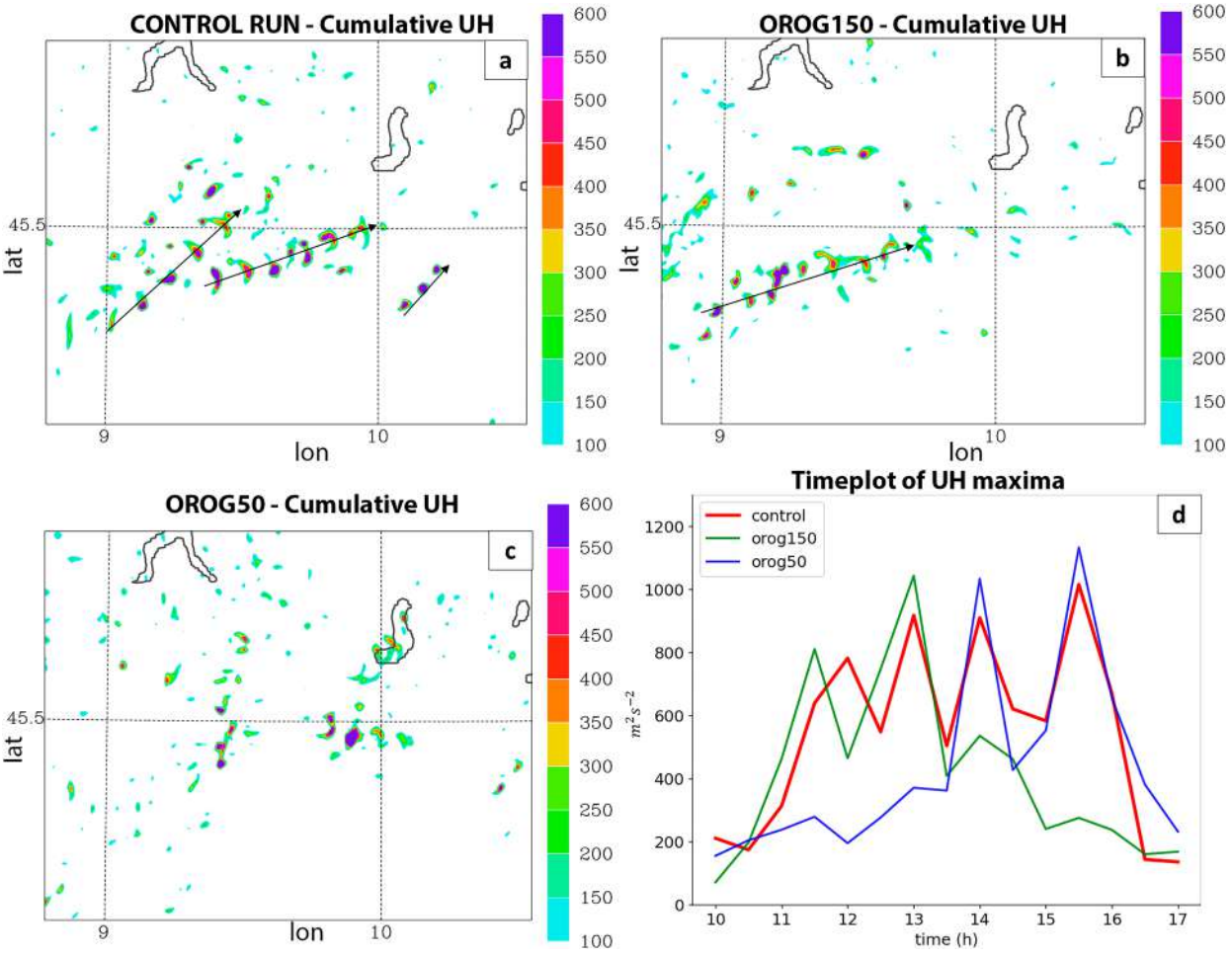

FIG. 10. (a) UH in the area indicated by the black box in Fig. 9, reported every 30 min between 0600 and 1800 UTC 19 Sep 2021. (a) Control run, (b) orog150 simulation, and (c) orog50 experiment. The supercell tracks are identified with black vectors. (d) Timeplot of the UH maxima for the three numerical experiments in the domain identified by a black box in Fig. 9.

sector, both MLCAPE (Fig. 13c) and MLCAPE 0–3 km (CAPE in the lowest 3 km of the atmosphere; Fig. 13e) peak to 1100 and 175 J kg^{-1}, respectively, while CIN (−15 J kg^{-1}; Fig. 13c) and the elevation of LCL and LFC (about 850 m; Fig. 13d) attain their lowest values. The peak of instability parameters corresponds to the peak of dewpoint temperature (Fig. 12a) and θ_e (Fig. 8) just ahead of the dryline. They were created by the advancement of the dryline (Figs. 8a,d,g), probably a consequence of a moisture pooling along the surface boundary (Johns 1993). In the numerical experiments orog50 and orog150, the same feature is observed, even if the duration of the period with peak values of θ_e is shorter and the location is different (Fig. 8), as discussed previously. This point is further clarified in Fig. 14, where the vertical profiles simulated by MOLOCH across the dryline show that the largest values of moisture in the PBL are 10 km ahead of it. South of the dryline, the instability parameters are not supportive for deep convection, due to the very dry air mass at the surface (Fig. 14a). Thirty kilometers ahead of the dryline, close to the Alpine foothills, the instability parameters rapidly decrease (Fig. 13c), due to a decrease in both moisture and temperature near the surface (Fig. 14c).

Not only the thermodynamic parameters change across the dryline but also the wind shear parameters. Ahead of the dryline, both SRH 0–3 km and SRH 0–1 km attain much higher values (respectively, about 200 and 130 $m^2 s^{-2}$) than behind. The values of SRH immediately ahead of the boundary and 30 km northward of it are similar (Fig. 13e). The difference between SRH 0–3 km and SRH 0–1 km is less than the value of SRH 0–1 km, thus indicating that the largest part of SRH 0–3 km is concentrated near the ground: This is a favorable condition for tornadic supercells (Rasmussen 2003). The larger values of wind shear just ahead of the dryline are due to the sharp veering of the wind from southeast near the surface to southwest above 1500 m, as can be observed from the simulated hodographs in Fig. 14.

Therefore, in the control run, the best combination of instability and directional wind shear is attained 10 km ahead of the dryline, where in fact there is a peak of STP and energy–helicity index (EHI; Hart and Korotky 1991). The values of

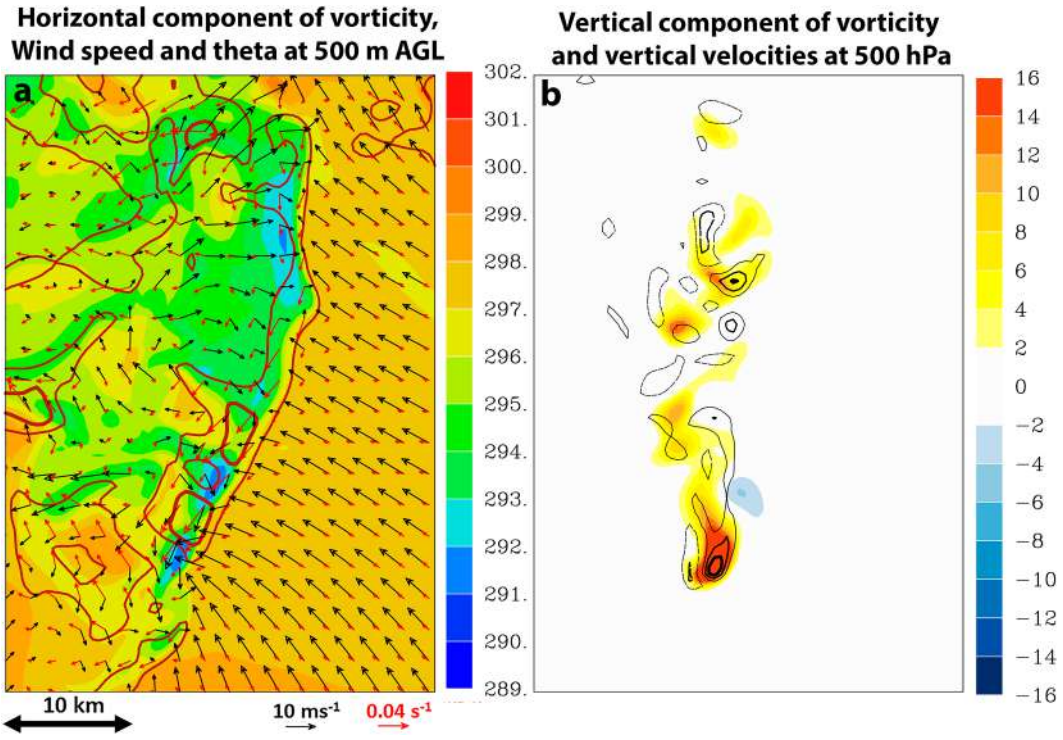

FIG. 11. (a) The θ (K; shaded), wind (black vectors), and horizontal component of vorticity [red vectors; red contours for 0.02 s^{-1} (thin line) and 0.04 s^{-1} (thick line) values] at 500 m AGL at 1330 UTC 19 Sep 2021; (b) vertical velocities (m s^{-1}; shaded) and vertical component of vorticity [contours for 0.005 s^{-1} (thinnest) and 0.01 s^{-1} and 0.015 s^{-1} (thickest) values] at 500 hPa at the same instant. The reference vectors for wind and vorticity are also provided. The plotted domain is highlighted with a blue box in Fig. 6a.

these composite indices overcome the lower bound for tornadic events in the United States only in a narrow path 10 km ahead of the dryline (Fig. 13f): The peak of STP equal to 1.0 is included between the 90th percentile (STP = 0.5) and the 75th percentile (STP = 1.4) of the distribution of STP during significant tornado events in the United States (Thompson et al. 2003). Actually, the strongest tornadoes developed just 10–20 km north of the dryline (Figs. 3 and 4). Hence, in the actual case the favorable conditions were probably also beyond the 10-km distance, but in any case within a 30-km distance.

So far, we have discussed the importance of the dryline to create the best combination of instability and wind shear in a narrow area, which was achieved thanks to the strong veering of the wind near the ground and the moisture pooling ahead of the surface boundary. These conditions would have been achieved even if the southwesterly flow had been moist instead of dry. Hence, one might wonder about the importance of the presence of dry air to generate favorable environments to tornadogenesis in the Po Valley. The numerical experiment bm60 (Table 2) investigates this aspect, increasing the specific humidity in the low–middle levels of the southerly flow impinging the Apennines range. As a consequence, the wind profile and the location of the convergence line are unperturbed with respect to the control run (Fig. 13b), but the θ_e values are higher in the lee of the Apennines and the θ_e horizontal gradient across the surface boundary is much weaker (a dryline cannot be identified anymore). The larger values of θ_e south of the surface boundary have the effect of producing an environment favorable for deep convection even south of the surface boundary itself, as shown by higher values of CAPE and lower values of CIN and LFC (Figs. 13c,d). Consequently, in this experiment, severe storms formed farther south than the control run (see S6 in the supplemental material). While in the control run isolated storms develop, in the bm60 scenario a QLCS sweeps the Po Valley. We think that the presence of dry air limited the interaction between convective cells, favoring the generation of isolated storms, more prone to become supercells (Bluestein and Parker 1993; Bluestein and Weisman 2000).

c. *Tornadic environment in ERA5*

As discussed in the introduction, ERA5 reanalysis (horizontal resolution of 0.25°) seems unsuitable to properly describe tornadic environments in the Po Valley. To verify this behavior, a comparison against the control high-resolution MOLOCH simulation (horizontal grid spacing of 500 m) is performed for this case study.

Figure 14 shows the vertical profiles and hodographs obtained from ERA5 and MOLOCH at specific locations with respect to the dryline. ERA5 and MOLOCH localize the convergence zone between southwesterly and southeasterly flows almost in the same position (not shown). ERA5 and MOLOCH hodographs have a similar shape, but the southeasterly flow is

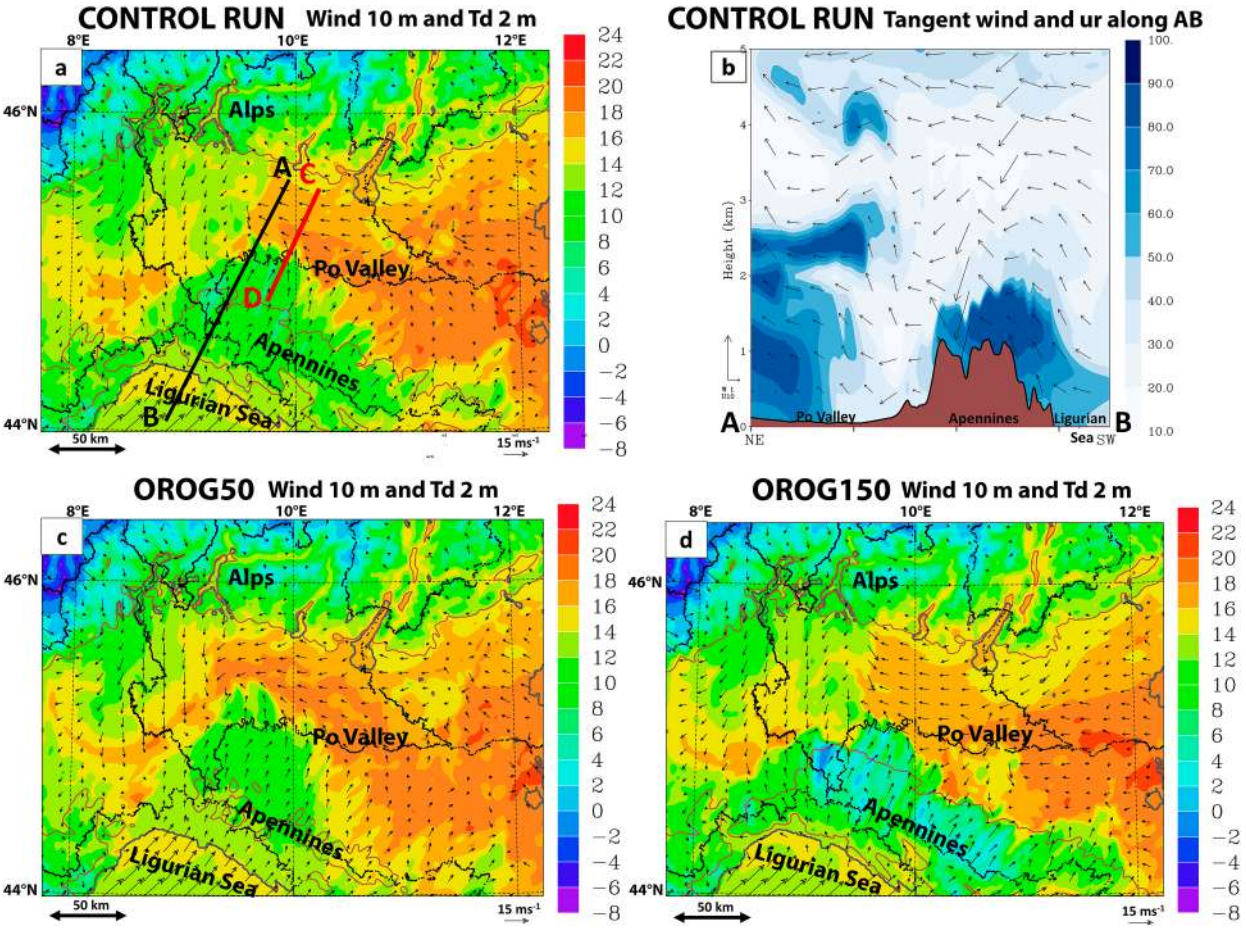

FIG. 12. Dewpoint temperatures (°C) at 2 m AGL (shaded) and wind vectors at 10 m AGL in (a) the control run, (c) orog50 experiment, and (d) orog150 experiment (1400 UTC 19 Sep 2021). In (b), the relative humidity and tangent wind vectors of the control simulation are plotted along the cross section AB shown in (a). The plotted domain is the same as in Fig. 6.

weaker in ERA5 and also the resulting SRH is lower. The differences between the dewpoint temperature vertical profiles are even more evident: ERA5 significantly underestimates the moisture pooling close to the dryline. The SB CAPE obtained from ERA5 is very low, and also, the LCL is higher. Probably, ERA5 resolution is too coarse to correctly represent environments favorable to tornado development in regions with such complex orography and strong inhomogeneities. A high-resolution numerical model can overcome these limitations, dramatically improving the representation of environmental conditions.

5. Discussion and conceptual model

Three different air flows interacted in the Po Valley during the tornadic outbreak that occurred on 19 September 2021: (i) a cool northerly flow from the Alps; (ii) a moist and warm easterly flow from the Adriatic Sea; and (iii) a dry southwesterly downslope flow from the Apennines. An outflow boundary was observed between the first two, while between (ii) and (iii) a dryline developed. We found that these two surface boundaries were crucial for the generation of the tornadic outbreak. The outflow boundary triggered a long-lived supercell (Fig. 3). Moreover, it likely generated streamwise vorticity along the gradient of potential temperature (Fig. 11), possibly intensifying the low-level mesocyclone. On the other hand, about 10 km north of the dryline, large amounts of moisture near the ground created a local peak of instability and a minimum LCL elevation (Figs. 13 and 14). In the same location, a strong veering with the heights of the winds from southeast to southwest generated large values of SRH (Figs. 13 and 14). The long-lived supercell moved inside the narrow stripe ahead of the dryline, where it encountered the best combination of instability and wind shear for the development of tornadoes, thus generating multiple F1+ tornadoes close to the triple point. The orientation of the narrow region with respect to the storm motion was a relevant feature, since it allowed the storms to reside in the favorable area for several hours.

We believe that significant tornadoes in the Po Valley may develop within this peculiar setup, since our results are in good agreement with B21. They similarly found that tornadic events in NE Italy are associated with cold air from the Alps (Figs. 15a,b), a dry (i.e., high LCL values; Figs. 15e,f) downslope flow from the Apennines (Figs. 15c,d), and an unstable

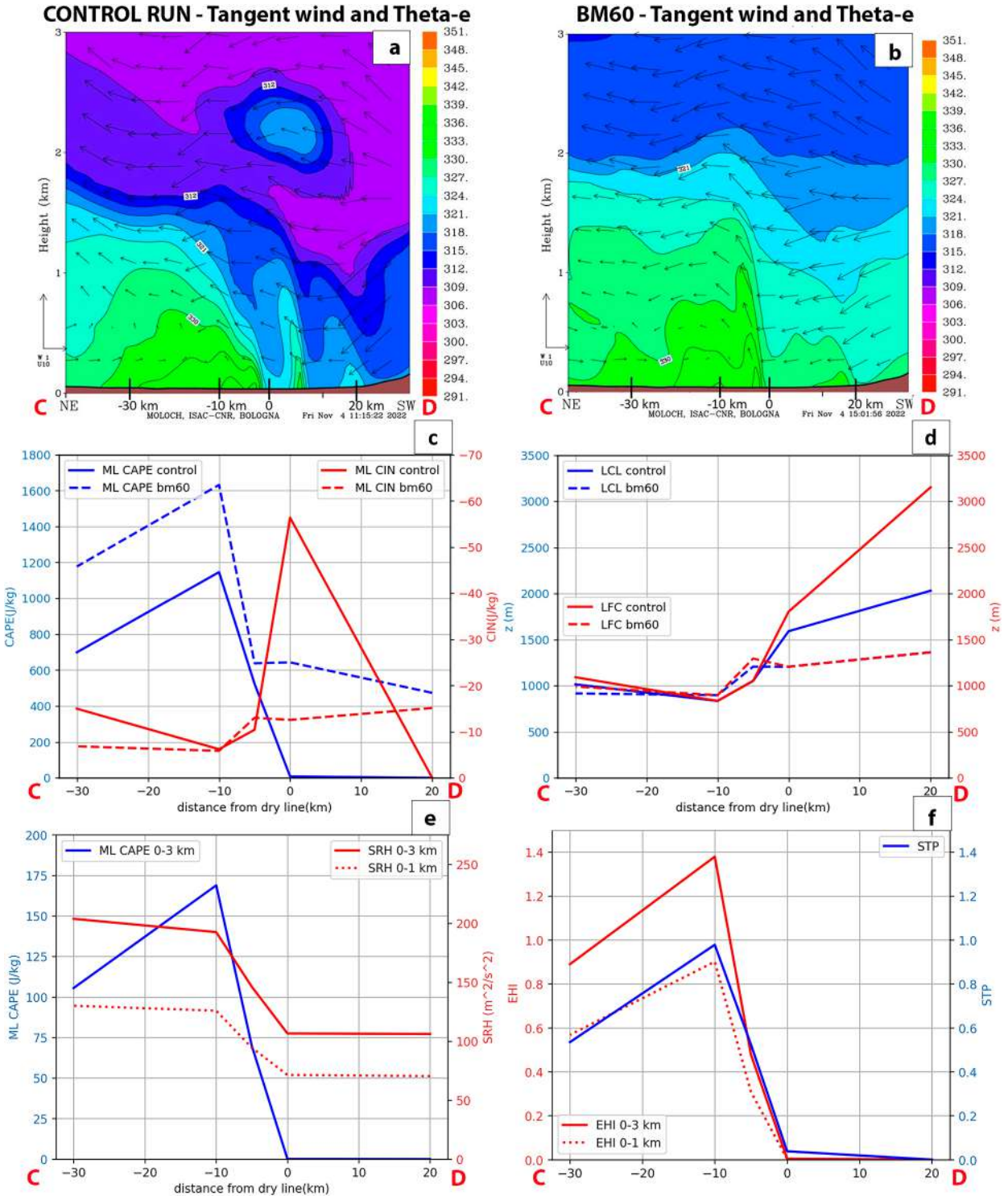

FIG. 13. Cross section at 1400 UTC 19 Sep 2021, along the red line CD in Fig. 12a: tangent wind (vectors) and θ_e (shaded) for (a) control run and (b) bm60 run. (c) MLCAPE (blue) and CIN (red) along the cross section for the control run (continuous line) and bm60 run (dashed line). (d) As in (c), but for LFC (red) and LCL (blue). (e) CAPE 0–3 km (blue), SRH 0–3 km (red solid line), and SRH 0–1 km (red dotted line) in the control run. (f) STP (blue line), EHI 0–3 km (red solid line), and EHI 0–1 km (red dotted line) for the control run. The x axis indicates the distance with respect to the dryline in Fig. 12a. Nearby parallel cross sections gave similar results.

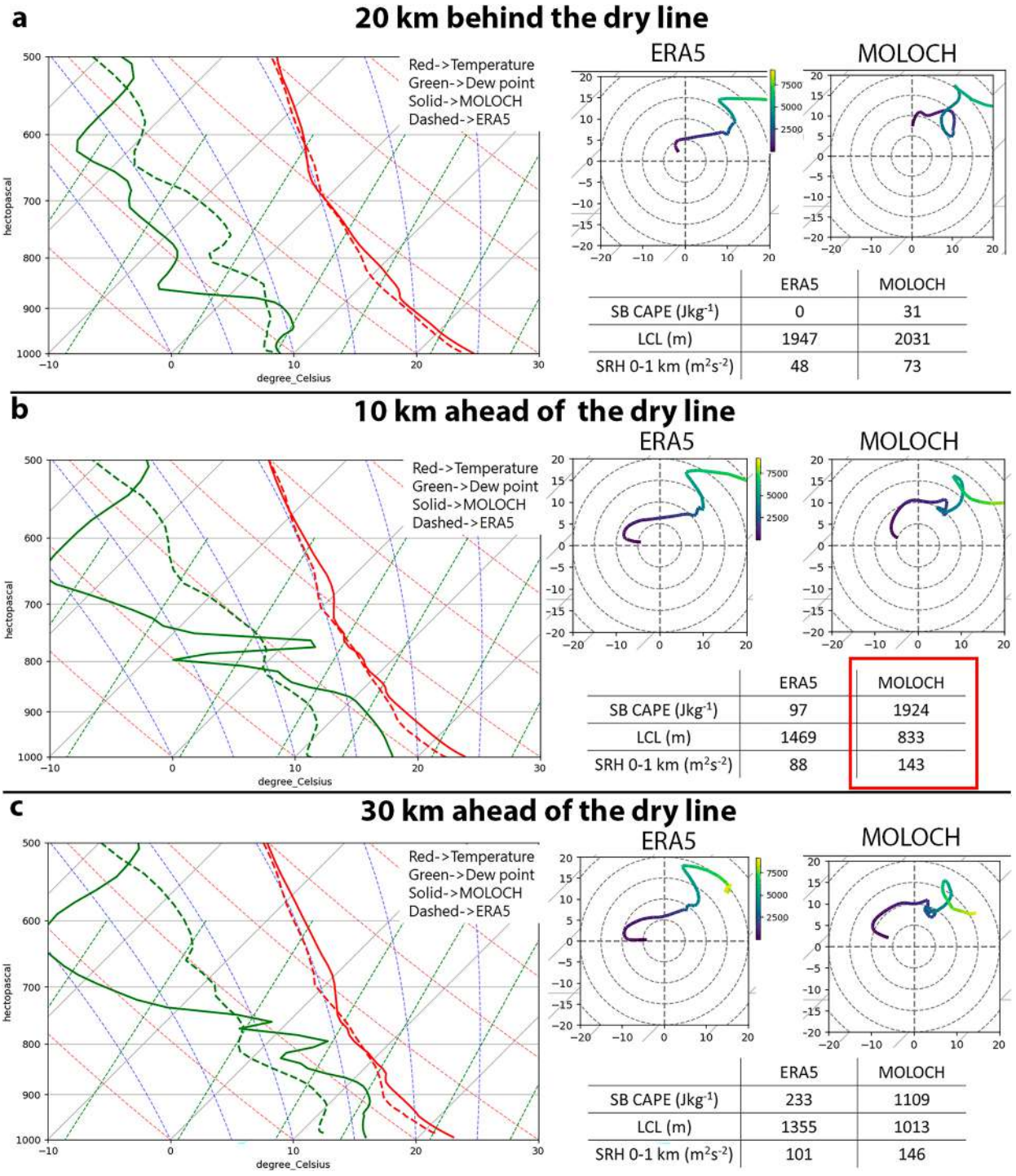

FIG. 14. Vertical profiles obtained from ERA5 (dashed) and simulated by MOLOCH (solid) at 1400 UTC 19 Sep 2021: (a) 20 km behind the dryline; (b) 10 km ahead of the dryline; (c) 30 km ahead of the dryline.

tongue from the Adriatic Sea (Figs. 15g,h). These features are consistent with the mesoscale environment observed during the 19 September 2021 event.

Hence, a conceptual model for the typical development of tornadoes in the Po Valley is proposed here (Fig. 16), extending the model of Miglietta et al. (2016) and adapting the one proposed for the U.S. Great Plains by Maddox et al. (1980) to the peculiarity of northern Italy. Severe storm events in the Po Valley are associated with a warm and moist air tongue, with high θ_e values and moderate SRH, which

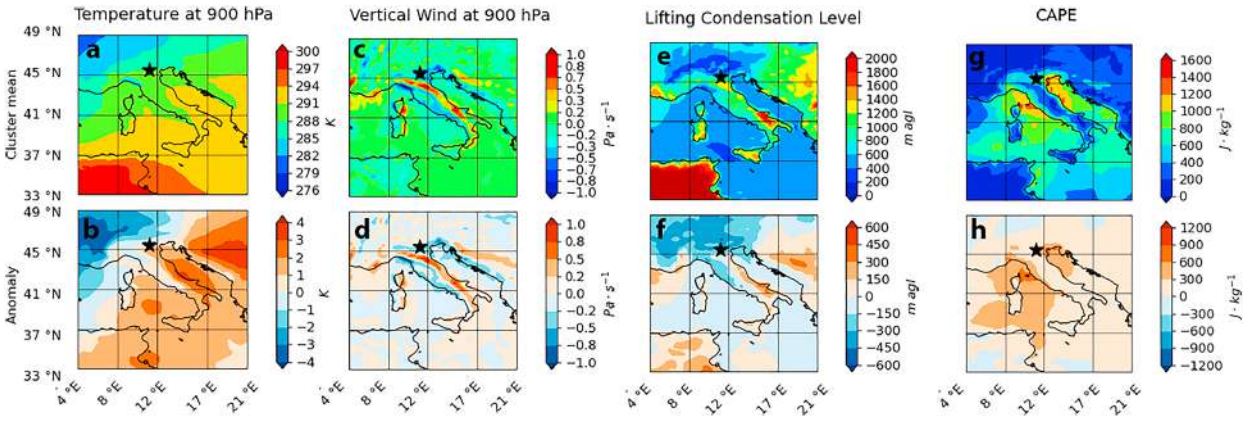

FIG. 15. ERA5 cluster mean (top) and anomaly (bottom) during tornadic events in NE Italy (the black star denotes the mean tornado location in the cluster NE). (a),(b) Temperature at 900 hPa; (c),(d) vertical wind component at 900 hPa; (e),(f) LCL; (g),(h) CAPE. Adapted from Figs. 5, 7, 11, and 13 of B21 [© Elsevier 2021, with permission].

enters the plain from the Adriatic Sea. Convection is initially triggered in the vicinity of the Alps (Manzato et al. 2022), and then, it propagates in the Po Valley sustained by outflow boundaries. Last, dry air descending from the Apennines generates a dryline, which may eventually trigger other isolated storms. The probability of the development of tornadoes is higher closer to the triple point generated by the intersection of the three different air masses, where local maxima of streamwise vorticity and instability are present near the surface.

6. Conclusions

The tornadic outbreak that affected the Po Valley on 19 September 2021 was thoroughly studied by means of observations and high-resolution numerical simulations. At the synoptic scale, the event was triggered by a cutoff low, which swept the Po Valley, associated with a strong upper-level PV anomaly and a jet streak. From an initial QLCS, a long-lived supercell developed, which lasted around 7 h. Two surface boundaries were observed: an outflow boundary, which moved eastward, and a dryline, which advanced slowly northeastward. The surface boundaries intersected at a triple point, similar to those observed in the U.S. Great Plains. In a few hours, seven tornadoes developed, always close to the triple point (typically around 20 km northeast of it), and four of them were rated as F2.

Using observations and high-resolution numerical simulations, the crucial role of surface boundaries was discussed and a conceptual model for the development of tornadoes in this region was proposed (Fig. 16). The conceptual model is

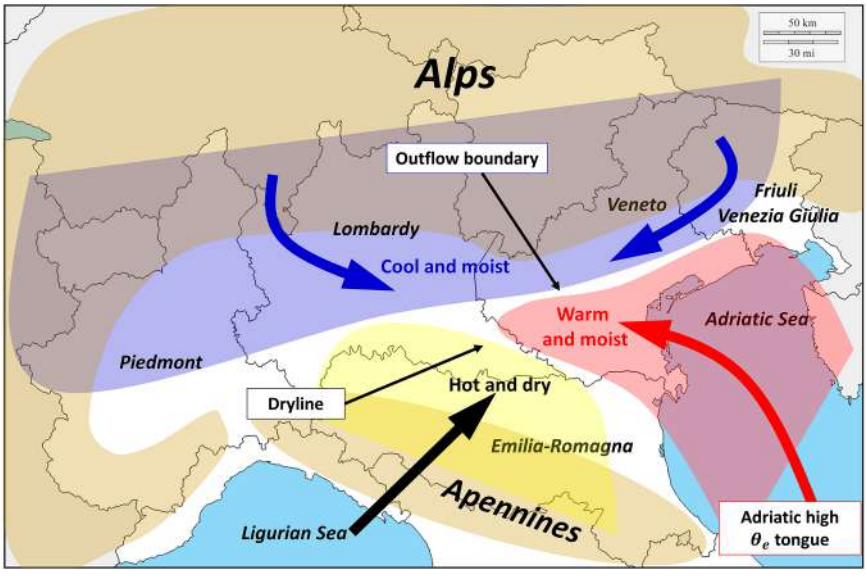

FIG. 16. Conceptual model of tornadoes setup in the Po Valley.

inspired by the work of Maddox et al. (1980), but there are some features that are peculiar to the Po Valley region, characterized by complex orography:

1) Convection is mainly initiated in the Alps (Manzato et al. 2022), and then, outflow boundaries propagate the storms in the plain. However, drylines may occasionally trigger isolated supercells directly in the plain (e.g., the Carpi storm in Fig. 4d), similarly to U.S. drylines (Bluestein and Parker 1993). Moreover, the dryline is generated by the advection of dry air mass from the southwest and by the adiabatic compression in the lee of the Apennines (Fig. 12), differently from the U.S. Great Plains where drylines are generated by the advection of continental air masses.
2) The development of supercells in the Po Valley is sensitive to the Apennines orography. The flow regime of the southwesterly flow crossing the Apennines can be diagnosed using the Froude number upstream, over the Ligurian Sea (Fig. 9).
3) The areal extension of surface boundaries associated with the triple point in the Po Valley is much smaller than that in the U.S. Great Plains, because mountain ridges delimit the horizontal extent of mesoscale boundaries (Fig. 4a).
4) The proper favorable conditions for tornado development in terms of moisture, instability, and wind shear near the ground are attained only in a narrow stripe close to the dryline. Even if the stripe is narrow, supercells can become tornadic if the storm motion allows them to reside for a sufficiently long time within the favorable area (Fig. 14).

This conceptual model may also explain the peak of tornado frequency in the Veneto region identified in Miglietta and Matsangouras (2018). In fact, in this region, the convergence of the three different air masses described in Fig. 16 is observed more frequently compared to the surrounding northern Italian regions. For example, the violent F4 tornado of Mira and Dolo on 8 July 2015 developed close to a triple point in a way very similar to that observed on 19 September 2021 (Abinanti et al. 2016).

Finally, this research points out why ERA5 was unable to reproduce the tornadic environment for this case study: It is likely that the horizontal resolution is too coarse to catch the small-scale features important for the development of tornadoes in the Po Valley. We think that this may explain the unusually low values of wind shear and instability obtained by B21 using ERA5 in tornado events in this region.

Future studies should verify this conceptual model in other case studies of violent tornadoes in the Po Valley, in order to consolidate our findings and to understand how frequently the identified pattern is observed on tornado days in this region. Finally, a study of drylines generated by the Apennines is necessary to better understand their relationship with the development of tornadoes from a climatological point of view.

Acknowledgments. We are grateful to Federico Cassola and Davide Sacchetti (ARPA Liguria) that provided SRH and reflectivity figures for the MOLOCH simulations for the generation of Figs. 6b, 6d, and 6f and the support for Figs. S3, S4, S5, and S6. We are also grateful to the Environmental Agencies of Emilia Romagna Region (ARPAE) and of Lombardy Region (ARPA Lombardia) for providing station data and interpolated surface observations; to the Weather Service of the Italian Military Air Force for providing Fig. S1; and to the Civil Protection Department of Italy for providing radar images and rainfall data. Richard Rotunno is acknowledged for his comments on the first draft of this paper. Three anonymous reviewers are gratefully acknowledged for their insightful comments on the first versions of the manuscript. PierPaolo Alberoni is acknowledged for checking the availability of some Doppler radar velocities for the event.

Data availability statement. Ground observations, provided by Regional Environmental Agencies, are available through the open-data web portals of ARPAE (https://dati.arpae.it/dataset) and Mistral (https://meteohub.mistralportal.it/app/datasets); soundings data are available at http://weather.uwyo.edu/upperair/europe.html (S. Pietro Capofiume Station WMO code is 16144); ERA5 reanalysis data are available through the Copernicus Climate Data Store at https://cds.climate.copernicus.eu; and IFS analysis used to describe the synoptic situation and to initialize the simulations is available through the Meteorological Archival and Retrieval System (MARS) of the European Centre for Medium-Range Weather Forecasts (ECMWF). MOLOCH simulation output is too large to be publicly archived with available resources, and data are archived locally and available upon request to the corresponding author.

REFERENCES

Abinanti, V., and Coauthors, 2016: Il tornado di Pianiga, Dolo e Mira Dell'8 Luglio 2015. Rep., 210 pp., https://www.fenomenitemporaleschi.it/tornado_8luglio2015_capitoli.pdf.

Antonescu, B., D. M. Schultz, A. Holzer, and P. Groenemeijer, 2017: Tornadoes in Europe: An underestimated threat. *Bull. Amer. Meteor. Soc.*, **98**, 713–728, https://doi.org/10.1175/BAMS-D-16-0171.1.

Atkins, N. T., M. L. Weisman, and L. J. Wicker, 1999: The influence of preexisting boundaries on supercell evolution. *Mon. Wea. Rev.*, **127**, 2910–2927, https://doi.org/10.1175/1520-0493(1999)127<2910:TIOPBO>2.0.CO;2.

Avolio, E., and M. M. Miglietta, 2021: Multiple tornadoes in the Italian Ionian regions: Observations, sensitivity tests and mesoscale analysis of convective storm environmental parameters. *Atmos. Res.*, **263**, 105800, https://doi.org/10.1016/j.atmosres.2021.105800.

——, and ——, 2022: Tornadoes in the Tyrrhenian regions of the Italian peninsula: The case study of 28 July 2019. *Atmos. Res.*, **278**, 106285, https://doi.org/10.1016/j.atmosres.2022.106285.

——, and ——, 2023: A comparative analysis of two Mediterranean tornado hotspots. *Atmosphere*, **14**, 189, https://doi.org/10.3390/atmos14010189.

Bagaglini, L., R. Ingrosso, and M. M. Miglietta, 2021: Synoptic patterns and mesoscale precursors of Italian tornadoes. *Atmos. Res.*, **253**, 105503, https://doi.org/10.1016/j.atmosres.2021.105503.

Bechis, H., J. Ruiz, P. Salio, M. Cancelada, and M. A. Imaz, 2022: Mesoscale influences on the development of a dryline in

Argentina: A modelling case study. *Atmos. Res.*, **265**, 105926, https://doi.org/10.1016/j.atmosres.2021.105926.

Bluestein, H. B., 2000: A tornadic supercell over elevated, complex terrain: The divide, Colorado, storm of 12 July 1996. *Mon. Wea. Rev.*, **128**, 795–809, https://doi.org/10.1175/1520-0493(2000)128<0795:ATSOEC>2.0.CO;2.

——, and S. S. Parker, 1993: Modes of isolated, severe convective storm formation along the dryline. *Mon. Wea. Rev.*, **121**, 1354–1372, https://doi.org/10.1175/1520-0493(1993)121<1354:MOISCS>2.0.CO;2.

——, and M. L. Weisman, 2000: The interaction of numerically simulated supercells initiated along lines. *Mon. Wea. Rev.*, **128**, 3128–3149, https://doi.org/10.1175/1520-0493(2000)128<3128:TIONSS>2.0.CO;2.

Bosart, L. F., A. Seimon, K. D. LaPenta, and M. J. Dickinson, 2006: Supercell tornadogenesis over complex terrain: The Great Barrington, Massachusetts, Tornado on 29 May 1995. *Wea. Forecasting*, **21**, 897–922, https://doi.org/10.1175/WAF957.1.

Buzzi, A., M. D'Isidoro, and S. Davolio, 2003: A case-study of an orographic cyclone south of the Alps during the MAP SOP. *Quart. J. Roy. Meteor. Soc.*, **129**, 1795–1818, https://doi.org/10.1256/qj.02.112.

——, S. Davolio, P. Malguzzi, O. Drofa, and D. Mastrangelo, 2014: Heavy rainfall episodes over Liguria in autumn 2011: Numerical forecasting experiments. *Nat. Hazards Earth Syst. Sci.*, **14**, 1325–1340, https://doi.org/10.5194/nhess-14-1325-2014.

Davolio, S., A. Volonté, A. Manzato, A. Pucillo, A. Cicogna, and M. Ferrario, 2016: Mechanisms producing different precipitation patterns over north-eastern Italy: Insights from HyMeX-SOP1 and previous events. *Quart. J. Roy. Meteor. Soc.*, **142**, 188–205, https://doi.org/10.1002/qj.2731.

——, R. Henin, P. Stocchi, and A. Buzzi, 2017: Bora wind and heavy persistent precipitation: Atmospheric water balance and role of air–sea fluxes over the Adriatic Sea. *Quart. J. Roy. Meteor. Soc.*, **143**, 1165–1177, https://doi.org/10.1002/qj.3002.

——, P. Malguzzi, O. Drofa, D. Mastrangelo, and A. Buzzi, 2020: The piedmont flood of November 1994: A testbed of forecasting capabilities of the CNR-ISAC meteorological model suite. *Bull. Atmos. Sci. Technol.*, **1**, 263–282, https://doi.org/10.1007/s42865-020-00015-4.

Feldmann, M., R. Rotunno, U. Germann, and A. Berne, 2024: Supercell thunderstorms in complex topography–how mountain valleys with lakes can increase occurrence frequency. *Mon. Wea. Rev.*, **152**, 471–489, https://doi.org/10.1175/MWR-D-22-0350.1.

Groenemeijer, P., and T. Kühne, 2014: A climatology of tornadoes in Europe: Results from the European severe weather database. *Mon. Wea. Rev.*, **142**, 4775–4790, https://doi.org/10.1175/MWR-D-14-00107.1.

Hart, J. A., and W. D. Korotky, 1991: The SHARP Workstation v. 1.50: A skew T/hodograph analysis and research program for the IBM and compatible PC: User's manual. NOAA/NWS Forecast Office, 62 pp.

Hersbach, H., and Coauthors, 2020: The ERA5 global reanalysis. *Quart. J. Roy. Meteor. Soc.*, **146**, 1999–2049, https://doi.org/10.1002/qj.3803.

Hoch, J., and P. Markowski, 2005: A climatology of springtime dryline position in the U.S. Great Plains region. *J. Climate*, **18**, 2132–2137, https://doi.org/10.1175/JCLI3392.1.

Homar, V., M. Gayà, R. Romero, C. Ramis, and S. Alonso, 2003: Tornadoes over complex terrain: An analysis of the 28th August 1999 tornadic event in eastern Spain. *Atmos. Res.*, **67–68**, 301–317, https://doi.org/10.1016/S0169-8095(03)00064-4.

Hubbard, M. E., and N. Nikiforakis, 2003: A three-dimensional, adaptive, Godunov-type model for global atmospheric flows. *Mon. Wea. Rev.*, **131**, 1848–1864, https://doi.org/10.1175//2568.1.

Ingrosso, R., P. Lionello, M. M. Miglietta, and G. Salvadori, 2020: A statistical investigation of mesoscale precursors of significant tornadoes: The Italian case study. *Atmosphere*, **11**, 301, https://doi.org/10.3390/atmos11030301.

Johns, R. H., 1993: Meteorological conditions associated with bow echo development in convective storms. *Wea. Forecasting*, **8**, 294–299, https://doi.org/10.1175/1520-0434(1993)008<0294:MCAWBE>2.0.CO;2.

Maddox, R. A., L. R. Hoxit, and C. F. Chappell, 1980: A study of tornadic thunderstorm interactions with thermal boundaries. *Mon. Wea. Rev.*, **108**, 322–336, https://doi.org/10.1175/1520-0493(1980)108<0322:ASOTTI>2.0.CO;2.

Malguzzi, P., G. Grossi, A. Buzzi, R. Ranzi, and R. Buizza, 2006: The 1966 "century" flood in Italy: A meteorological and hydrological revisitation. *J. Geophys. Res.*, **111**, D24106, https://doi.org/10.1029/2006JD007111.

Manzato, A., S. Serafin, M. M. Miglietta, D. Kirshbaum, and W. Schulz, 2022: A pan-alpine climatology of lightning and convective initiation. *Mon. Wea. Rev.*, **150**, 2213–2230, https://doi.org/10.1175/MWR-D-21-0149.1.

Markowski, P. M., and N. Dotzek, 2011: A numerical study of the effects of orography on supercells. *Atmos. Res.*, **100**, 457–478, https://doi.org/10.1016/j.atmosres.2010.12.027.

——, and Y. P. Richardson, 2014: The influence of environmental low-level shear and cold pools on tornadogenesis: Insights from idealized simulations. *J. Atmos. Sci.*, **71**, 243–275, https://doi.org/10.1175/JAS-D-13-0159.1.

——, E. N. Rasmussen, and J. M. Straka, 1998: The occurrence of tornadoes in supercells interacting with boundaries during vortex-95. *Wea. Forecasting*, **13**, 852–859, https://doi.org/10.1175/1520-0434(1998)013<0852:TOOTIS>2.0.CO;2.

Matsangouras, I. T., P. T. Nastos, and I. Pytharoulis, 2016: Study of the tornado event in Greece on March 25, 2009: Synoptic analysis and numerical modeling using modified topography. *Atmos. Res.*, **169**, 566–583, https://doi.org/10.1016/j.atmosres.2015.08.010.

May, R. M., and Coauthors, 2022: MetPy: A meteorological python library for data analysis and visualization. *Bull. Amer. Meteor. Soc.*, **103**, E2273–E2284, https://doi.org/10.1175/BAMS-D-21-0125.1.

Miglietta, M. M., and R. Rotunno, 2016: An EF3 multivortex tornado over the Ionian region: Is it time for a dedicated warning system over Italy? *Bull. Amer. Meteor. Soc.*, **97**, 337–344, https://doi.org/10.1175/BAMS-D-14-00227.1.

——, and I. T. Matsangouras, 2018: An updated "climatology" of tornadoes and waterspouts in Italy. *Int. J. Climatol.*, **38**, 3667–3683, https://doi.org/10.1002/joc.5526.

——, A. Manzato, and R. Rotunno, 2016: Characteristics and predictability of a supercell during HyMeX SOP1. *Quart. J. Roy. Meteor. Soc.*, **142**, 2839–2853, https://doi.org/10.1002/qj.2872.

——, J. Mazon, V. Motola, and A. Pasini, 2017a: Effect of a positive sea surface temperature anomaly on a Mediterranean tornadic supercell. *Sci. Rep.*, **7**, 12828, https://doi.org/10.1038/s41598-017-13170-0.

——, ——, and R. Rotunno, 2017b: Numerical simulations of a tornadic supercell over the Mediterranean. *Wea. Forecasting*, **32**, 1209–1226, https://doi.org/10.1175/WAF-D-16-0223.1.

Morcrette, J.-J., H. W. Barker, J. N. S. Cole, M. J. Iacono, and R. Pincus, 2008: Impact of a new radiation package, McRad, in the ECMWF integrated forecasting system. *Mon. Wea. Rev.*, **136**, 4773–4798, https://doi.org/10.1175/2008MWR2363.1.

Pavan, F., 2022: Eventi tornadici Dell'Autunno 2021: 19/09. PRETEMP Rep., 113 pp., https://www.pretemp.it/archivio/2022/studi_2022/19settembre.pdf.

Pichelli, E., R. Rotunno, and R. Ferretti, 2017: Effects of the Alps and Apennines on forecasts for Po valley convection in two HyMeX cases. *Quart. J. Roy. Meteor. Soc.*, **143**, 2420–2435, https://doi.org/10.1002/qj.3096.

Pilguj, N., M. Taszarek, M. Kryza, and H. E. Brooks, 2022: Reconstruction of violent tornado environments in Europe: High-resolution dynamical downscaling of ERA5. *Geophys. Res. Lett.*, **49**, e2022GL098242, https://doi.org/10.1029/2022GL098242.

Poli, V., and R. Stanzani, 2021: Rapporto dell'evento meteorologico del 19 e 20 Settembre 2021. Agenzia Regionale per la Protezione dell'Ambiente dell'Emilia Romagna Rep., 23 pp., https://allertameteo.regione.emilia-romagna.it/documents/20181/437770/Evento+19-20+settembre+2021.pdf/ff3ed88f-773d-06e9-eb02-d0a306ae9121?t=1633503536867.

Púčik, T., P. Groenemeijer, D. Rýva, and M. Kolář, 2015: Proximity soundings of severe and nonsevere thunderstorms in central Europe. *Mon. Wea. Rev.*, **143**, 4805–4821, https://doi.org/10.1175/MWR-D-15-0104.1.

Rasmussen, E. N., 2003: Refined supercell and tornado forecast parameters. *Wea. Forecasting*, **18**, 530–535, https://doi.org/10.1175/1520-0434(2003)18<530:RSATFP>2.0.CO;2.

——, S. Richardson, J. M. Straka, P. M. Markowski, and D. O. Blanchard, 2000: The association of significant tornadoes with a baroclinic boundary on 2 June 1995. *Mon. Wea. Rev.*, **128**, 174–191, https://doi.org/10.1175/1520-0493(2000)128<0174:TAOSTW>2.0.CO;2.

Ritter, B., and J. F. Geleyn, 1992: A comprehensive radiation scheme for numerical weather prediction models with potential applications in climate simulations. *Mon. Wea. Rev.*, **120**, 303–325, https://doi.org/10.1175/1520-0493(1992)120<0303:ACRSFN>2.0.CO;2.

Rose, S. F., P. V. Hobbs, J. D. Locatelli, and M. Stoelinga, 2004: A 10-yr climatology relating the locations of reported tornadoes to the quadrants of upper-level jet streaks. *Wea. Forecasting*, **19**, 301–309, https://doi.org/10.1175/1520-0434(2004)019<0301:AYCRTL>2.0.CO;2.

Rotunno, R., and J. Klemp, 1985: On the rotation and propagation of simulated supercell thunderstorms. *J. Atmos. Sci.*, **42**, 271–292, https://doi.org/10.1175/1520-0469(1985)042<0271:OTRAPO>2.0.CO;2.

Signani, M., 2021: Incredibile supercella tornadica fra Cremona e Brescia, 19 Settembre 2021.Accessed 11 February 2023, https://www.stormnetwork.it/2021/09/21/incredibile-supercella-tornadica-fra-cremona-e-brescia-19-settembre-2021/.

Taszarek, M., J. T. Allen, P. Groenemeijer, R. Edwards, H. E. Brooks, V. Chmielewski, and S. Enno, 2020a: Severe convective storms across Europe and the United States. Part I: Climatology of lightning, large hail, severe wind, and tornadoes. *J. Climate*, **33**, 10 239–10 261, https://doi.org/10.1175/JCLI-D-20-0345.1.

——, ——, T. Púčik, K. A. Hoogewind, and H. E. Brooks, 2020b: Severe convective storms across Europe and the United States. Part II: ERA5 environments associated with lightning, large hail, severe wind, and tornadoes. *J. Climate*, **33**, 10 263–10 286, https://doi.org/10.1175/JCLI-D-20-0346.1.

Thompson, R. L., R. Edwards, J. A. Hart, K. L. Elmore, and P. Markowski, 2003: Close proximity soundings within supercell environments obtained from the rapid update cycle. *Wea. Forecasting*, **18**, 1243–1261, https://doi.org/10.1175/1520-0434(2003)018<1243:CPSWSE>2.0.CO;2.

Tochimoto, E., and H. Niino, 2016: Structural and environmental characteristics of extratropical cyclones that cause tornado outbreaks in the warm sector: A composite study. *Mon. Wea. Rev.*, **144**, 945–969, https://doi.org/10.1175/MWR-D-15-0015.1.

——, M. M. Miglietta, L. Bagaglini, R. Ingrosso, and H. Niino, 2021: Characteristics of extratropical cyclones that cause tornadoes in Italy: A preliminary study. *Atmosphere*, **12**, 180, https://doi.org/10.3390/atmos12020180.

Trini Castelli, S., A. Bisignano, A. Donateo, T. C. Landi, P. Martano, and P. Malguzzi, 2020: Evaluation of the turbulence parametrization in the MOLOCH meteorological model. *Quart. J. Roy. Meteor. Soc.*, **146**, 124–140, https://doi.org/10.1002/qj.3661.